***Title*: Divergent neuronal DNA methylation patterns across human cortical development: Critical periods and a unique role of CpH methylation**

Authors

Price AJ[1,2]*, Collado-Torres L[1,3]*, Ivanov NA[1], Xia W[1], Burke EE[1], Shin JH[1], Tao R[1], Ma L[1], Jia Y[1], Hyde TM[1,4,5], Kleinman JE[1,5], Weinberger DR[1,2,4,5,6], Jaffe AE[1,2,3,7,8,+]

Affiliations

1. Lieber Institute for Brain Development, Johns Hopkins Medical Campus, Baltimore, MD, USA
2. McKusick-Nathans Institute of Genetic Medicine, Johns Hopkins University School of Medicine, Baltimore, MD, USA
3. Center for Computational Biology, Johns Hopkins University, Baltimore, MD, USA
4. Department of Neurology, Johns Hopkins School of Medicine, Baltimore, MD, USA
5. Department of Psychiatry, Johns Hopkins School of Medicine, Baltimore, MD, USA
6. Department of Neuroscience, Johns Hopkins School of Medicine, Baltimore, MD, USA
7. Department of Mental Health, Johns Hopkins Bloomberg School of Public Health, Baltimore, MD, USA
8. Department of Biostatistics, Johns Hopkins Bloomberg School of Public Health, Baltimore, MD, USA

*equally contributing authors

Corresponding Author: Andrew E Jaffe, 855 N Wolfe St, Ste 300; Baltimore MD 21205.

Phone: 1-443-287-6864; Email: andrew.jaffe@libd.org

Abstract

We have characterized the landscape of DNA methylation (DNAm) across the first two decades of human neocortical development in NeuN+ neurons using whole-genome bisulfite sequencing and compared them to non-neurons (primarily glia) and prenatal homogenate cortex. We show that DNAm changes more dramatically during the first five years of postnatal life than during the entire remaining period. We further refined global patterns of increasingly divergent neuronal CpG and CpH methylation (mCpG and mCpH) into six developmental trajectories and found that in contrast to genome-wide patterns, neighboring mCpG and mCpH levels within these regions were highly correlated. We then integrated paired RNA-seq data and identified direct regulation of hundreds of transcripts and their splicing events exclusively by mCpH levels, independently from mCpG levels, across this period. We finally explored the relationship between DNAm patterns and development of brain-related phenotypes and found enriched heritability for many phenotypes within DNAm features we identify.

Introduction

Neurons are unique cells that persist throughout the lifespan, accumulating programmed developmental changes and environmental experience that fine tune neural circuitry in the brain. During development and maturation, neurons undergo precisely coordinated cascades of genetic regulation that combine with experience to shape the cellular output via progressive changes to the epigenome. DNA methylation (DNAm) is an integral facet of the epigenome that plays a role in establishing cell identity and developmental trajectories as well as adapting to experience via regulation of gene expression. Previous large-scale studies of DNAm across human brain development have been limited to homogenate tissue[1] or have used microarray technologies[2], creating ambiguity about the extent of cell type-specific developmental DNAm changes and effects on transcript isoforms across the genome[3].

To better characterize the DNAm landscape across human cortical development, we performed whole-genome bisulfite sequencing (WGBS, see Methods) on homogenate tissue and on a neuron-enriched population isolated from 24 human dorsolateral prefrontal cortex (DLPFC) samples aged 0-23 years using NeuN-based fluorescence-activated nuclear sorting (FANS, **Figure S1A**). To complement these data, we sequenced eight FANS-derived NeuN- postnatal samples and 20 homogenate prenatal cortical samples, for a total of 75 samples after quality control (**Table S1**). We fully characterized the landscape of DNAm at both CpG and non-CpG (CpH) dinucleotides in these samples, allowing for a finer dissection of differential DNAm functional specificity. We also sequenced matched transcriptomes of homogenate cortical samples from these donors and a subset of three nuclear transcriptomes each from NeuN+ and NeuN- samples to assess the functional consequences of epigenomic remodeling (53 total transcriptomes, **Table S2**). By exploring DNAm patterns in neurons across prenatal and postnatal human brain development, we show that the first five years of postnatal life are a

critical period in epigenetic plasticity, and we identify developmental shifts in neuronal DNAm in both the CpG and CpH context. We also clarify the relationship between CpG but particularly CpH methylation (mCpG and mCpH, respectively) and gene expression and splicing in neuronal development, and explore the ramifications of these insights for neuropsychiatric disease.

Results

After data processing, quality control and filtering, we analyzed 18.7 million cytosines in the CpG context at an average coverage of 15x (see methods). Comparable to previous reports[1,4,5], CpGs were overall highly methylated (71-76% CpGs with β>80%, **Table S3**).

While NeuN antibody labels most mature neuronal subtypes in human cortex, some neurons will not be labeled and will be captured in the NeuN- fraction amidst a diverse array of non-neuronal cell types, including oligodendrocytes, astrocytes, microglia, and epithelial cells. Gene expression differences between fractions confirmed, however, that NeuN+ and NeuN- samples are enriched for neuronal and glial-lineage cells, respectively (**Figure S1B-D**). Therefore in this work we refer to NeuN+ and NeuN- samples as “neurons” and “glia” although we acknowledge that these samples do not perfectly reflect these identities and mask more granular differences between subcellular identities contained within.

Developmental DNAm changes identified in homogenate cortex were strongly confounded by shifting cell type proportions (OR=7.5, $p<10^{-100}$, **Figure S2A**)[2]. While homogenate measurements were positively correlated with developmental changes that occurred in both neuronal and glial cell types (ρ=0.79, $p<10^{-100}$), cell type-specific developmental changes were less consistently observed in homogenate preparations (ρ=-0.26, $p<10^{-100}$, **Figure S2B-D**). Overall, ~40% of cell type-specific developmental DNAm changes could not be detected at all in homogenate cortex (**Figure S2E**), and many of the cell type-specific effects

81 could not be accurately identified in homogenate tissue. These results highlight the importance
82 of measuring DNAm in the appropriate cellular context for improved resolution to detect true
83 developmental changes.

84 *DNAm as a map of putative functional genomic states*

85 Local CpG methylation (mCpG) patterns are known to distinguish genomic states of
86 DNA and chromatin. For instance, unmethylated regions (UMRs) are associated with promoters,
87 with a subset of longer UMRs (DNAm valleys, DMVs) that overlap developmental genes often
88 encoding transcription factors (TFs)[6,7]; low-methylated regions (LMRs) often signify enhancer
89 sequence[8]; and partially methylated domains (PMDs) are associated with heterochromatin and
90 late replicating DNA[9–11]. To better resolve the developing regulatory landscape in postnatal
91 neurons and glia and in bulk prenatal cortex, we assessed the temporal dynamics of these
92 selected DNAm patterns in the CpG context. Compared to prenatal homogenate cortex and
93 postnatal glial cells, postnatal neurons showed a general accumulation of mCpG, at a rate 50%
94 faster than the other cells. This was evident in the LMR and to a lesser extent the UMR
95 landscape, since fewer and smaller LMRs were identified as neuronal development progressed
96 (**Figure S3A-B**). As expected, UMRs and LMRs were highly enriched for transcription start sites
97 (TSSs) and enhancers in DLPFC chromatin state data from the Roadmap Epigenomics
98 Consortium[12] (**Figure S3C**). Interestingly, LMRs were similarly enriched in these states in both
99 adult and fetal brain; this correspondence may reflect a shared regulatory landscape established
100 early in development.

101 While PMDs are a common feature of most cell types, they have not been conclusively
102 identified in neurons. Here we identified a range of 245 to 404 PMDs per neuronal sample
103 (**Figure S4A**). PMDs were especially enriched for heterochromatin and, interestingly, enhancers

104 in our postnatal neuronal samples (**Figure S4B**). 65.4% of PMD base pairs were also identified
105 as PMD in an independent WGBS dataset of NeuN-sorted human neurons (**Figure S4C**).
106 40.3-61.0% of PMD bases per neuronal sample were identified as common PMD sequence, and
107 9.3-15.0% bases were additionally identified as PMD in at least one sample in a recent study
108 profiling PMDs in multiple cell types and tissues[13] (**Figure S4D**). These data suggest that
109 although the neuronal genome was overall highly methylated, a small but consistent portion
110 displayed the characteristics of PMDs.

111 We further identified significant neuronal DMV changes through accumulation of mCpG
112 that revealed regulators of cell identity and development and their temporal windows of
113 expression change. Compared to bulk prenatal cortex, postnatal neurons and glia showed
114 marked reduction in the size of DMVs (**Figure S5A**). Methylation shifts within DMVs led to
115 inclusion and exclusion of transcription factor genes in an age-dependent manner, and on
116 average transcription factor genes were higher expressed in the age group in which the gene
117 was escaping the DMV state by accumulating DNAm (**Figure S5B-C**). These results underscore
118 the substantial DNAm landscape alterations that neurons and glia undergo during development
119 in defined mCpG patterns, including previously unobserved PMDs.

120 *Developmental shifts in neuronal mCpG highlight synaptic remodeling during first five years of*
121 *postnatal life*

122 We next quantified more localized changing mCpG levels by exploiting the correlation
123 between neighboring mCpG levels to identify genomic regions with changing mCpG. We
124 identified 11,179 differentially methylated regions (DMRs, FWER<5%, see Methods) in the CpG
125 context between cell types (covering 31.1 Mb) that replicated in independent WGBS data[1]
126 (98.4% concordant, ρ=0.925, **Figure S6A**). Many of these DMRs overlapped genes involved in

127 neuronal or glial-specific processes (**Figure S6B**). We found fewer DMRs for developmental
128 mCpG changes compared with cell type differences, the majority being within rather than across
129 cell types (2,178 versus 129 DMRs, at ~5% change in DNAm per decade of life, FWER<5%).
130 Among the 2,178 cell type-specific developmental DMRs (cdDMRs, 3 Mb, **Table S4**), neuronal
131 mCpG patterns seemed to diverge from an immature landscape shared by glia and prenatal
132 cortex (**Figure 1A**), with the largest changes occuring in the first five years of life. Indeed, the
133 magnitude of DNAm changes in neurons and glia in samples five years and younger was double
134 that of older samples (**Figure S6C-D**). These results provide epigenetic correlates to the known
135 developmental processes occuring in the cortex in the first five postnatal years, including prolific
136 synaptogenesis and gliogenesis.

137 We further parsed these cdDMRs using k-means clustering to partition the cdDMRs into
138 six groups with unique DNAm characteristics (**Figure 1B**). 71.1% of cdDMRs were in groups
139 characterized by increasing neuronal and/or decreasing glial DNAm over postnatal development
140 (**Figure 1B;** Groups 1, 2 & 6). A varying proportion of each cdDMR group corresponded to
141 sequence differentially methylated by neuronal subtype from publicly available data[14] depending
142 on the trajectory of neuronal methylation patterns in the group, suggesting that assorted
143 neuronal subclasses contribute to these developmental patterns (**Figure S7A-B**). Gene
144 ontology enrichment in the six groups suggested that these groups are associated with a
145 continuum of biological roles, many relating to functions specific to the cell type with decreasing
146 methylation (**Figure 1C**). For example, **Figure 1D** shows a Group 3 cdDMR within *SNAP25*, a
147 presynaptic neuronal gene, in which neurons uniquely and progressively lost DNAm over
148 development. This pattern suggests increased repression of a neuronal fate in maturing glia not
149 mirrored in neurons over postnatal development in Group 3 cdDMRs. Likewise, the opposite
150 pattern was observed in a Group 6 cdDMR within *MBP*, an oligodendrocyte gene encoding a

151 component of the myelin sheath, in which glia but not neurons progressively lost DNAm (**Figure**
152 **1E**).

153 We lastly compared these cdDMR groups to a list of putative enhancers active in human
154 brain development curated by evolutionary age[15] and found strong enrichment for these
155 sequences across all six groups (**Figure S8A**). Human accelerated regions, or conserved
156 sequences that have experienced rapid mutation in the human lineage[16], were also enriched for
157 dynamic DNAm remodeling (**Figure S8B**), suggesting that our CpG-based cdDMRs may be
158 enriched for sequences related to higher cognitive functions associated with the human DLPFC.

159 Overlapping cdDMRs with the mCpG features identified above provided additional
160 insight to the potential functional genomic states underlying these regions. For instance,
161 cdDMRs scarcely overlapped heterochromatic PMDs; cdDMRs losing neuronal mCpG were
162 positively correlated with increasing LMR overlap, potentially reflecting enhancer element
163 activation during cortical maturation in these groups (Groups 3 & 5 cdDMRs; both with $t>3.8$,
164 $\rho>0.63$, and FDR<2.7e-03). Curiously, a high proportion of cdDMRs gaining DNAm in glia but
165 not in neurons (Group 4 cdDMRs) overlapped DMVs early in development in glia but steadily
166 lost DMV status over time ($t=-4.3$, $\rho=-0.87$, FDR=1.3e-02, **Figure S9A**). Assessing chromatin
167 state from the homogenate Roadmap Epigenomics brain maps, in contrast, lacked the
168 resolution to provide this nuance: all six cdDMR groups were similarly enriched for
169 transcriptional (particularly TSS-flanking) and enhancer chromatin states, and depleted for
170 heterochromatin and quiescent states (**Figure S9B**). These results confirm the role of dynamic
171 DNAm in helping establish epigenomic states that guide cell lineage differentiation and
172 emphasize the utility of creating genome-wide DNAm maps to better parse the functional
173 diversity of cell type-specific developmental DNAm remodeling in the human cortex, a process
174 that is particularly critical during the first five years of postnatal development.

175 *Abundant neuronal CpH methylation is highly correlated with neighboring CpG methylation*

176 Unlike in most other somatic tissues and cell types, mCpH is an abundant, conserved
177 feature of the neuronal epigenome[1,4]. We therefore analyzed 58.1 million cytosines in CpH
178 contexts (H=A,T, or C) that had evidence of methylation across the samples (coverage ≥5, at
179 least 5 samples with β>0, see Methods). As shown previously[1], mCpH sites were predominantly
180 lowly methylated (92-99% CpHs with β<20%, **Table S3**). While mCpH was distributed
181 throughout the genome (**Figure S10A**), it was greater in neurons than glia (98.9% of 7,682,075
182 differentially methylated CpHs were in neurons, at FDR<5%) and mostly accumulated across
183 postnatal development (99.3% of 3,194,618 CpHs, at FDR<5%; **Table S5**). Most mCpH
184 accumulated primarily in either the CAG or CAC context over the first five years of postnatal
185 life—similarly to mCpG—followed by a tapered global increase into adulthood (**Figure S10B**).

186 While the majority of mCpH in embryonic stem cells (ESCs) occurs in the CAG context,
187 previous work has shown that ESCs undergo loss of mCAG during neuronal differentiation
188 followed by preferential accumulation of mCAC[17]. Here we further refined these patterns and
189 found a cell type-specific relationship with trinucleotide context: overall, total mCAG increased
190 40% faster than mCAC in neurons, while in glia, mCAG accumulated 50% slower than mCAC
191 (**Figure S10C**). Taking into account relative genome-wide proportions of CAG and CAC though,
192 neuronal mCAG accumulated 30% slower than mCAC (**Figure 2A**). mCH that was greater in
193 glia than neurons, or in younger than older neurons, was more likely to be in the CAG than CAC
194 context (OR>4.13, p<2.2e-16). Interestingly, the 3,286 and 1,744 genes that contained
195 significantly increasing and decreasing mCAC versus mCAG over development, respectively,
196 were associated with different biological processes related to neuronal function and activity,
197 particularly involving the synapse (**Figure S10D**). These results reinforce that trinucleotide

198 context may be regulated by distinct mechanisms playing non-redundant biological roles in
199 human brain development.

200 We next examined the relationship between neighboring mC levels by measuring
201 autocorrelation, or how correlated the methylation level of a cytosine is with that of cytosines
202 progressively further away. Unlike in the CpG context, where neighboring mCpG levels were
203 highly correlated as previously described[18], neighboring CpH DNAm levels across the genome
204 were not autocorrelated. Within the cdDMRs, however, while mCpH levels separately remained
205 uncorrelated, together all methylated cytosines (i.e., mCpH+mCpG) showed similar
206 autocorrelation as mCpG levels alone (**Figure 2B**). This was especially surprising given that
207 there were about two times as many CpHs than CpGs within these regions and that the CpG
208 and CpH were relatively interspersed, suggesting potential functional convergence in the
209 developmentally regulated patterns identified by mCpG in these regions. Indeed, unsupervised
210 hierarchical clustering of CpH within the cdDMRs showed infant neuronal mCpH levels were
211 even more similar to glia compared to older neurons than mCpG (**Figure 2C**). Examining the
212 mean mCpH compared to mCpG within the k-means cdDMR clusters showed that the groups
213 gaining mCpG were the most correlated with mCpH trajectories within the cdDMRs (ρ=0.97,
214 t=17.6, p=2.0e-14), and that although mCpG (unlike mCpH) is present at high levels prenatally,
215 both mCpG and mCpH accumulate at similar rates over postnatal development in these groups,
216 once again especially in the first five years of postnatal life where the majority of the methylation
217 change takes place (t=-0.091, p=0.94; **Figure S11**). These results emphasize the potential
218 regulatory importance of cdDMRs and putative functional agreement between both contexts of
219 DNAm in these regions.

220 *mCpG and mCpH levels influence transcript isoform use*

221 Previous studies show that both mCpG and mCpH in gene bodies but particularly in the
222 promoter and first 2 kb of the gene are negatively associated with gene expression, and that
223 genic mCpH is the most discriminating predictor of gene expression[1,5]. To anchor our DNAm
224 patterns in transcriptional activity, we compared our WGBS data with NeuN-sorted nuclear
225 RNA-seq data (see Methods). We took the average DNAm levels across six groups—infant
226 (ages 0-1), child (ages 1-10), and teen (age 10+) within both cell types (neuronal and
227 glial)—and calculated associations between DNAm and expression. Gene expression was
228 negatively correlated with mCpG regardless of age and cell type in both promoter sequence and
229 gene bodies ($-0.42<\rho<-0.22$, p~0; 57,332 genes, $p < 10^{-100}$; **Figure S12A**). Interestingly, mCpG
230 in exons was significantly but weakly positively correlated with exon expression in infancy,
231 particularly in glial samples ($\rho=0.094$, $p < 10^{-100}$), which may relate to the previously-identified
232 positive relationship between mCpG and expression and higher methylation in exons than
233 introns[9].

234 Across promoters, gene bodies, and exons, only neurons showed a negative correlation
235 between gene expression and mCpH, a relationship that became stronger over development
236 (**Figure S12B**). This pattern was consistent with the preferential accumulation of mCpH in
237 neurons as the brain matures. mCAC and mCAG showed similar patterns of increasingly strong
238 negative correlation preferentially in neurons between methylation and expression across these
239 features (**Figure S12C-D**). Both mCpG and mCpH surrounding exon-exon splice junctions were
240 weakly negatively correlated with expression of the junction in neurons (**Figure S12E**).

241 Because mCpG has previously been associated with alternative splicing[19] and mCpH is
242 15-20% greater in exons than in introns[9], we hypothesized that accumulating mCpH may
243 contribute to the diversity of alternative splicing characteristic of the brain particularly during
244 development. Leveraging our single-base resolution data, we were able to identify genome-wide

245 functional correlates of mCpH, independent of nearby mCpG, by associating DNAm with nearby
246 expression in the same cortical samples. Specifically, we tested whether methylation levels
247 directly associated with gene or exon expression levels as well as the “percent spliced in” (PSI)
248 of alternative splicing events using the 22 neuronal samples with matching homogenate polyA+
249 RNA-seq data (see Methods). We found 40,940 CpG and 40,303 CpH associations that explain
250 changes in these three expression summarizations at FDR<5% with a genome-wide $p<5x10^{-4}$.
251 We further identified 220,622 marginal ($p<0.01$) CpG associations with expression within 1 kb
252 around the associated CpH. While an independent association of mCpH at the gene and PSI
253 summarizations was rare, there were substantially more exons exclusively regulated by local
254 mCpH, largely in the CHH context, in developing postnatal neurons (**Figure 3A**). Three
255 examples of methylation-associated isoform changes are shown in **Figure 3B**.

256 Regardless of context specificity, these expression-associated cytosines were depleted
257 in gene promoters and instead enriched in gene bodies and flanking regions (**Table 1**, see
258 Methods). Both contexts were enriched for the high-GC 3’ and 5’ canonical splice site
259 sequences (FDR<1.1e-04), although the associated cytosine could be either inside or outside
260 the corresponding expression feature. Only 3.5-13.7% of expression-associated cytosines
261 overlapped DMR sequence after stratifying by expressed feature and dinucleotide context,
262 indicating that these associations may arise from a more individualized mC effect than the
263 DMRs.

264 Although the majority of these DNAm-expression associations were independent of
265 development despite being identified in developing neurons, the mCpH changes at these sites
266 were independently associated with age and expression. The genes including PSI events
267 regulated by local DNAm levels in both CpG and CpH contexts were consistently enriched for
268 neuronal components (**Figure S13**), while genes containing methylation-associated alternative

269 exons were enriched for synaptic signaling and neurotransmitter transport (**Figure 3C** and
270 **Figure S14**), suggesting that we are detecting true neuronal mC-expression associations
271 despite measuring splicing in homogenate RNA-seq. Many of these genes were also
272 differentially expressed between neuronal and glial nuclear RNA (FDR<0.05, **Table 1**). Most, but
273 not all, expression-associated cytosines at the gene- and exon-level showed significant
274 decreases in expression as methylation levels increased.

275 The associations between these putatively regulatory cytosines and nearby expression
276 levels can be explored in a webtool (https://jhubiostatistics.shinyapps.io/wgbsExprs/). Results
277 can be interactively summarized such as in **Table 1** for user-selected subsets and visualized as
278 in **Figure 3B** or via the UCSC genome browser (**Figure S15**). By integrating neuronal mCpG
279 and mCpH levels with accompanying RNA-seq data in the same brains, we have identified, for
280 the first time, direct regulation of hundreds of transcripts and their splicing events exclusively by
281 mCpH, independent of mCpG levels, across the first two decades of human cortical
282 development.

283 *DNAm patterns shed light on the active cell type and timing of neuropsychiatric phenotype*
284 *development*

285 Previous work has attributed a high proportion of neuropsychiatric trait heritability to
286 neuron-specific DNA methylation patterns[20]. Given the role of dynamic DNAm in marking DNA
287 sequence function over development, we examined the relationship between our methylation
288 features with heritability for 30 human behavioral-cognitive traits, psychiatric and neurological
289 disorders, and non-brain-related traits[21] (**Table S6**), hypothesizing that DNAm patterns may
290 illuminate not only the active cell type but potential critical timeframes for genomic activity in
291 these complex phenotypes. We used stratified linkage disequilibrium score regression (LDSC)[22]

292 to estimate the proportion of heritability measured in GWAS summary statistics for each
293 phenotype that could be attributed to each of 16 genomic features, including 10 sets of DMRs,
294 LMRs identified in the prenatal, glial or neuronal methylome, human brain regulatory sequence
295 annotated by chromHMM or the LDSC package, or non-differential CpG clusters (**Figure 4A**). In
296 agreement with previous findings[20,23], human brain annotated regulatory sequence was broadly
297 enriched for heritability of brain-specific traits (14 of 26 brain-associated phenotypes enriched in
298 chromHMM or CNS (LDSC) regions at FDR≤0.05), as were neuronal features (10 of 26 brain
299 phenotypes enriched in neuronal hypomethylated regions, FDR≤0.05; **Table S7**). Significantly
300 differentially hypomethylated neuronal regions had on average 1.85 times higher enrichment
301 scores than non-differential neuronal LMRs, meaning the DMRs explained 1.85x more
302 heritability over regions containing a similar number of SNPs than the LMRs. Interestingly, body
303 mass index (BMI) heritability was enriched in general brain regulatory sequence and
304 hypomethylated neuronal DMRs (FDR≤0.05), consistent with previous evidence linking this
305 metabolic phenotype to regulatory sequence active in cells of the human central nervous
306 system[22].

307 In terms of developmental DNAm patterns, heritability of BMI, IQ, neuroticism, and major
308 depressive disorder was enriched in both postnatal neuronal and prenatal LMRs, suggesting
309 early action of genetic influence on the development of these phenotypes (FDR≤0.05). Few
310 developmental differential groups captured a significant proportion of heritability for the 30 traits
311 tested, perhaps because of their small size compared to the cell type-specific or non-differential
312 groups (cdDMRs covered ~31, 240 and 838 times less sequence and included ~32, 273 and
313 904 times fewer SNPs than cell type DMRs, LMRs or general brain features, respectively).
314 However, despite covering only 607 kilobases, group 3 cdDMRs (ie, static glial and decreasing
315 neuronal DNAm) were significantly enriched for heritability of schizophrenia (coefficient

316 z-score=2.74, FDR=0.039). Group 4 cdDMRs (111.7 kilobases; increasing glial, static neuronal
317 DNAm) were also enriched for heritability of PTSD (coefficient z-score=3.21, FDR=0.01).
318 Given the enrichment for psychiatric disease heritability measured in common SNPs in
319 these cdDMR groups, we then expanded our analysis to include seven curated gene sets
320 containing *de novo* and rare inherited variation--including rare copy number variants (CNVs) and
321 syndromic variants--associated with psychiatric, neurodevelopmental and neurodegenerative
322 disorders[24,25]. We again found significant enrichment of hypomethylated neuronal DMRs in
323 genes implicated in psychiatric and neurodevelopmental disorders (i.e., schizophrenia, autism
324 spectrum disorder (ASD), syndromal neurodevelopmental disorders, and intellectual disability;
325 all with OR>2.04 and FDR<1.9e-02; **Table S8**). In this analysis, we also found enrichment for
326 hypermethylated neuronal DMRs in ASD genes from the SFARI Gene database and
327 schizophrenia genes containing *de novo* mutations (both with OR>1.92 and FDR<5.0e-03).
328 These results confirmed a prominent role of neuronal functioning in most of the
329 neurodevelopmental disorders using an orthogonal measurement approach as done
330 previously[23]. Over postnatal development, Group 5 cdDMRs (increasing glial, decreasing
331 neuronal DNAm) were enriched in ASD genes from the SFARI Gene database (OR=5.7,
332 FDR=4.1e-03), while Group 6 cdDMRs (decreasing glial, static neuronal DNAm) were enriched
333 in ASD, syndromal neurodevelopmental disorder, and intellectual disability genes (all with
334 OR>3.1 and FDR<1.9e-02). In contrast, a curated set of neurodegenerative disorder genes
335 showed no enrichment for cdDMRs, perhaps reflecting lesser relevance of the first two decades
336 of postnatal epigenomic remodeling to the etiology of those disorders.
337 In the non-CpG context, we found significant enrichment of both increasing and
338 decreasing mCpH levels in genes associated with schizophrenia, ASD, and syndromal
339 neurodevelopmental disorders (all with OR>2.1 and FDR<2.0e-02). CpH hypomethylation in

340 neurons was also enriched in the neurodegenerative disease gene set (OR=2.6, FDR=3.7e-03).
341 Finally, significantly increasing mCpH was depleted in genes associated with intellectual
342 disability (OR=0.34, FDR=3.7e-06). While enrichment for conflicting mCpH patterns are at first
343 curious given the overall negative association between mCpH and gene expression, outside of
344 the context of DMRs, individual mCpH could be associated both positively and negatively with
345 expression. Indeed, many genes, exons, and PSI events whose expression both positively and
346 negatively associated with both mCpH and mCpG were also enriched in genes associated with
347 schizophrenia, ASD, and syndromal neurodevelopmental disorders (all with OR>2.1 and
348 FDR<2.5e-02; **Table S9**). Overall these results suggest that these examples of dynamic
349 methylation and associated isoform switching may play a role in the development of higher
350 cognitive functions during brain maturation associated with these diseases.

351 **Discussion**

352 Here we have created a single-base resolution map of the dynamic DNAm landscape
353 across the first two decades of postnatal human brain development in two cell type-enriched
354 populations. Using FANS-derived samples, we were able to identify 40% more
355 developmentally-regulated regions of changing DNAm than were identified in homogenate
356 DNAm cortical data. We profiled specific features of the DNAm landscape including LMRs,
357 UMRs, PMDs and DMVs and found that across features, neurons were typified by a general
358 accumulation of mCpG. In the absence of complementary cell type-specific chromatin data,
359 characterizing known DNAm features provided a more granular view of the potential functional
360 genomic state in these regions than the available predictions derived from a few homogenate
361 cortical samples. Particularly in studies using human postmortem brain, where tissue is often
362 subjected to long postmortem intervals and low pH that degrades less stable epigenetic

363 signatures, DNAm is a robust and durable marker that can be used to map the functional
364 genomic terrain. These DNAm maps complement recently available epigenomic maps of
365 different modalities generated on FANS-derived samples in the psychENCODE Consortium[27].
366 We further parsed the general accumulation of neuronal DNAm into six trajectories of
367 cell type-specific developmental patterns and found that neuronal mCpG progressively diverged
368 from a shared landscape with glia and bulk prenatal cortex as the brain matured. Importantly,
369 these diverging patterns were most striking during infancy through the first five years of
370 postnatal life. The human brain experiences an explosion of synaptic connections during this
371 time period, to nearly double the number found in the mature adult brain[28]. Although previous
372 work has underscored this timeframe in terms of rapid DNAm accumulation[1], this is the first
373 work to refine DNAm patterns to reflect cell type-specific gain and loss of mCpG and mCpH
374 within this critical window. By parsing these neuronal and glial DNAm patterns, we have
375 highlighted epigenetically dynamic regions that may be contributing to the developmental
376 processes such as synaptogenesis occuring during this timeframe that establish the foundation
377 for fine-tuning connections throughout the remainder of brain maturation. These results provide
378 a finely resolved depiction of epigenetic plasticity being greatest during this period of life, and
379 support other evidence that environmental experience during these years may have an
380 especially enduring impact on brain function[29].
381 mCpH is unusually abundant in neurons compared to other cell types and appears to
382 undergo trinucleotide-specific reprogramming during differentiation from ECSs[17]. While most
383 mCpH in ESCs occurs in the CAG context, neuronal mCpH predominantly accumulates in the
384 CAC context[17]. Here we elaborate on this relationship, showing that while both mCAG and
385 mCAC aggregate in neurons as they mature and mCAG is gained faster than mCAC overall,
386 mCAC accumulates proportionally faster in both neurons and glia over time. Interestingly,

387 although neurons and glia contained mCpH in both trinucleotide contexts, mCAG was more
388 likely to have higher levels in glia than neurons or be decreasing over development; indeed,
389 genes containing decreasing mCAG but not mCAC were strongly associated with neuronal
390 biological processes. mCpH trinucleotide context, therefore, may have as yet not well
391 understood ramifications in brain development.

392 In terms of the relationship between mCpH and mCpG, we found that while neighboring
393 mC (i.e., mCpG+mCpH) was not correlated genome-wide, mC was highly correlated within the
394 cdDMRs despite local mCpH not being correlated. In other words, there was a convergence of
395 levels of all contexts of methylation within the cdDMRs that was not detected genome-wide.
396 mCpH also recapitulated the pattern seen in mCpG of diverging from a shared DNAm
397 landscape with glia. Given that mCpH and mCpG have previously been shown to work in
398 concert to recruit MECP2 binding to fine-tune gene expression[30], it is sensible that levels of both
399 contexts would perhaps reflect a shared functional role within putatively regulatory cdDMR
400 sequence, since cdDMRs were also enriched for gene bodies and brain enhancer sequence.
401 This work quantifies this correlation for the first time, a DNAm relationship unique to only a
402 selection of cell types that includes neurons.

403 The identification of widespread association of mCpG and mCpH with expression and
404 specific splicing events, particularly in neuronal genes enriched for neuropsychiatric diseases,
405 highlights a potential novel role of mCpH and further expands the role of mCpG in the regulation
406 of gene expression in neurons. Splicing is predominantly a co-transcriptional process influenced
407 by changes in chromatin modifications and RNA binding proteins; the effects of DNAm on
408 splicing decisions is not yet well studied[31]. Here we found thousands of associations between
409 mC levels and gene, exon and PSI expression in developing postnatal neurons, particularly
410 featuring many exons that are exclusively associated with mCpH. Although it is not possible to

411 establish a causal role for mC in these data, these analyses, which are summarized in the
412 provided website, can empower other researchers to explore the connection between DNAm
413 and alternative isoform use, a phenomenon particularly prevalent in the developing brain that is
414 often associated with disease[32].

415 We also explored the relationship between DNAm patterns and genetic associations with
416 various phenotypes and found both expected and surprising associations. We confirmed
417 enrichment for heritability of brain traits generally in neurons, and heritability for schizophrenia, a
418 disorder with strong neurodevelopmental underpinnings, specifically in genomic regions losing
419 DNAm preferentially in neurons over early postnatal development (ie, Group 3 cdDMRs). This
420 result emphasizes the critical nature of neuronal development and maturation in early
421 establishment of pathological connectivity and function for this adult-onset disorder, as most
422 DNAm loss--generally associated with increased activity of a gene or regulatory
423 element--occurred within the first five postnatal years. Indeed, Group 3 cdDMRs were present in
424 genes such as *GRIN1*, *SYN1* and *CAMK2A*, and others involved in establishing synapse
425 organization and function, a hallmark of early postnatal brain development, implicating abnormal
426 genetic regulation of neuronal connectivity in schizophrenia development. Interestingly,
427 heritability for PTSD was significantly enriched in regions preferentially gaining DNAm in the
428 non-neurons over development (Group 4 cdDMRs), regions associated with neural precursor
429 cell proliferation and cell-cell connective properties (Figure 1C). This association, particularly
430 given the small amount of sequence covered by Group 4 cdDMRs, could lead to fruitful insights
431 into susceptibility for PTSD and warrants further study.

432 We also found enrichment of genes associated with rare variants implicated in
433 psychiatric and neurodevelopmental disease in a variety of cell types and developmental
434 trajectories, highlighting the the genomic boundaries, developmental timing and cellular context

435 of epigenomic remodelling of regulatory elements or expressed features associated with known
436 risk genes. Two examples of this are *HDAC4* and *CACNA1B,* genes associated with ASD in the
437 SFARI Gene database. We identified a 566 bp Group 3 (decreasing neuronal, static glial DNAm)
438 cdDMR within an intron of *HDAC4*, a calcium-sensitive transcriptional repressor, and a 3.6 kb
439 Group 5 (decreasing neuronal, increasing glial DNAm) cdDMR within *CACNA1B*, a gene
440 encoding a voltage-gated calcium channel subunit (**Figure 4B-C)**. Even though both genes are
441 implicated in ASD and both cdDMRs are hypomethylated in neurons, the timing of loss of mCpG
442 suggests that *CACNA1B* activity occurs earlier in postnatal development than *HDAC4*. Given
443 that ASD onset is typically in early childhood, these risk genes may therefore have differing
444 implications in the etiology of ASD. Another example is a 646 bp Group 6 (decreasing glial,
445 static neuronal DNAm) cdDMR that overlaps the last intron and exon of *AKT3*, a
446 serine/threonine-protein kinase gene. Although the *AKT3*/1q44 locus has been associated with
447 schizophrenia risk, the mechanisms are not yet known given that *AKT3* is involved in many
448 biological functions[25]. Interestingly, this cdDMR selectively lost mCpG in glia beginning in
449 infancy, suggesting that *AKT3* activity in human DLPFC may be localized to glia beginning in
450 infancy or earlier (**Figure 4D**). This work provides the first *ex vivo* look at the DNAm dynamics
451 within human neurons and glia and thus allows for the first examination of those parameters
452 within the relevant organ, the brain.

453 Despite these insights, our data invoke several caveats. While NeuN based FANS
454 greatly improves identifying developmental DNAm changes over homogenate data, designating
455 NeuN+ and NeuN- samples as “neurons” and “glia” is not completely accurate in that NeuN-
456 samples will include signal from unlabeled neurons and mask non-neuronal diversity. However,
457 recent work assessing brain regional DNAm differences between NeuN+ and NeuN- found that
458 NeuN- contributed comparatively marginal variability in DNAm compared to NeuN+, suggesting

459 that neuronal methylomes are much more dynamic than non-neurons[20]. Likewise, while a
460 percentage of the bases in the DMRs identified in this work have also been previously shown to
461 be differentially methylated by neuronal subtypes whose unique methylomes are masked using
462 NeuN-based FANS[5,14,33], the proportion of these subtypes should be stable over postnatal
463 development[34]. Future epigenomics studies however can improve on the resolution of our study
464 by isolating more specific neuronal subpopulations to refine the cellular specificity of these
465 neuronal methylation changes largely occurring in the first few years of life.

466 Another caveat is that WGBS does not allow for the discrimination between mC and
467 hydroxymethyl-cytosines (hmC), an intermediary in the demethylation pathway. Previous work
468 has shown[5] that only a fraction of CpGs have measurable levels of hmC, suggesting that our
469 results are not confounded. In the cited study[5], hmCpG signal from homogenate cortex
470 represented 10% of the hypermethylation found in excitatory neuron mCpG, suggesting that
471 most of the mCpG signal in our neuronal data likely is true mCpG. The level of hmC in the
472 non-CpG context remains controversial, with some studies not identifying hmCpH[5] and others
473 detecting low amounts (1% in FANS-derived human glutamatergic and 0.47% in GABAergic
474 neurons)[35]. Further, FANS-derived human oligodendrocytes showed little hmC in the same
475 study[35]. Overlap of our cdDMRs with DMRs between neurons and oligodendrocytes in a study of
476 mC in FANS-derived human PFC samples[32] showed that cell type differences primarily reflected
477 true mC rather than hmC contamination in WGBS, while hmC DMRs between neuronal
478 subtypes primarily were reflected in hypomethylated neuronal cdDMR groups and not the
479 hypermethylated neuronal groups that would potentially include hmC signal contamination
480 (**Figure S7B**). Future work, however, should more closely examine the contribution of hmC to
481 the global hypermethylation seen during neurodevelopment.

By mapping the changing DNAm landscape over human postnatal neuronal and glial development, we have identified unique trajectories of DNAm change particularly dynamic during the first five years of life that show convergence between mCpG and mCpH, as well as associations between single mCpG and mCpH and alternative splicing. These patterns may also help illuminate the mechanisms through which psychological, neurological and psychiatric traits are developed by placing known genetic contribution in an epigenomic context.

Acknowledgements

Author Contributions

- A.J.P.: Conceptualization, Formal Analysis, Investigation, Visualization, Writing – Original Draft Preparation, Writing – Review & Editing.
- L.C.-T.: Conceptualization, Formal Analysis, Visualization, Software, Writing – Original Draft Preparation, Writing – Review & Editing.
- N.A.I.: Software, Data Curation.
- W.X.: Investigation.
- E.E.B.: Formal Analysis, Writing – Review & Editing.
- J.H.S.: Supervision.
- R.T.: Investigation.
- L.M.: Investigation.
- Y.J.: Investigation, Supervision.
- T.M.H.: Data Curation, Resources, Writing – Review & Editing.
- J.E.K.: Data Curation, Resources, Writing – Review & Editing.
- D.R.W.: Conceptualization, Funding Acquisition, Supervision, Writing – Review & Editing.

- A.E.J.: Conceptualization, Formal Analysis, Funding Acquisition, Supervision, Writing – Original Draft Preparation, Writing – Review & Editing.

Funding

This project was supported by The Lieber Institute for Brain Development and by NIH grants R21MH102791, R21MH105853, and R01MH112751. Data were generated as part of the PsychENCODE Consortium, supported by: U01MH103392, U01MH103365, U01MH103346, U01MH103340, U01MH103339, R21MH109956, R21MH105881, R21MH105853, R21MH103877, R21MH102791, R01MH111721, R01MH110928, R01MH110927, R01MH110926, R01MH110921, R01MH110920, R01MH110905, R01MH109715, R01MH109677, R01MH105898, R01MH105898, R01MH094714, P50MH106934 awarded to: Schahram Akbarian (Icahn School of Medicine at Mount Sinai), Gregory Crawford (Duke University), Stella Dracheva (Icahn School of Medicine at Mount Sinai), Peggy Farnham (University of Southern California), Mark Gerstein (Yale University), Daniel Geschwind (University of California, Los Angeles), Fernando Goes (Johns Hopkins University), Thomas M. Hyde (Lieber Institute for Brain Development), Andrew E. Jaffe (Lieber Institute for Brain Development), James A. Knowles (University of Southern California), Chunyu Liu (SUNY Upstate Medical University), Dalila Pinto (Icahn School of Medicine at Mount Sinai), Panos Roussos (Icahn School of Medicine at Mount Sinai), Stephan Sanders (University of California, San Francisco), Nenad Sestan (Yale University), Pamela Sklar (Icahn School of Medicine at Mount Sinai), Matthew State (University of California, San Francisco), Patrick Sullivan (University of North Carolina), Flora Vaccarino (Yale University), Daniel R. Weinberger (Lieber Institute for Brain Development), Sherman Weissman (Yale University), Kevin White (University

of Chicago), Jeremy Willsey (University of California, San Francisco), and Peter Zandi (Johns Hopkins University).

Competing Interest

The funders had no role in study design, data collection and analysis, decision to publish, or preparation of the manuscript. Conflict of Interest: none declared.

Data availability

Raw and processed sequence data that support the findings of this study have been deposited at www.Synapse.org with the accession code: syn5842535.

Code availability

Code is available through GitHub at: https://github.com/LieberInstitute/brain-epigenomics.

Methods

Postmortem brain tissue acquisition and processing

As previously described in Jaffe *et al.* (2016)[2], post-mortem human brain tissue was obtained by autopsy primarily from the Offices of the Chief Medical Examiner of the District of Columbia, and of the Commonwealth of Virginia, Northern District, all with informed consent from the legal next of kin (protocol 90-M-0142 approved by the NIMH/NIH Institutional Review Board). Additional post-mortem prenatal, infant, child and adolescent brain tissue samples were provided by the National Institute of Child Health and Human Development Brain and Tissue Bank for Developmental Disorders (http://www.BTBank.org) under contracts NO1-HD-4-3368 and

546 NO1-HD-4-3383. Postmortem human brain tissue was also provided by donation with informed
547 consent of next of kin from the Office of the Chief Medical Examiner for the State of Maryland
548 (under Protocol No. 12-24 from the State of Maryland Department of Health and Mental
549 Hygiene) and from the Office of the Medical Examiner, Department of Pathology, Homer Stryker,
550 M.D. School of Medicine (under Protocol No. 20111080 from the Western Institute Review
551 Board). The Institutional Review Board of the University of Maryland at Baltimore and the State
552 of Maryland approved the protocol, and the tissue was donated to the Lieber Institute for Brain
553 Development under the terms of a Material Transfer Agreement. Clinical characterization,
554 diagnoses, and macro- and microscopic neuropathological examinations were performed on all
555 samples using a standardized paradigm, and subjects with evidence of macro- or microscopic
556 neuropathology were excluded, as were all subjects with any psychiatric diagnoses. Details of
557 tissue acquisition, handling, processing, dissection, clinical characterization, diagnoses,
558 neuropathological examinations, and quality control measures have also been further described
559 previously[36]. Homogenate postmortem tissue of the prefrontal cortex (dorsolateral prefrontal
560 cortex, DLPFC, BA46/9) was obtained from all subjects.

561 *Fluorescence activated nuclei sorting*

562 Nuclei were isolated from 100-300mg of pulverized DLPFC tissue using dounce homogenization
563 followed by ultracentrifugation over a sucrose density gradient. Homogenization was performed
564 on ice in 5mL lysis buffer [0.32M sucrose, 3mM magnesium acetate, 5mM calcium chloride,
565 5mM EDTA (ph 8.0), 10mM Tris-HCl (pH 8.0), 0.1% Triton X-100] and the resulting homogenate
566 was layered over 38mL sucrose buffer [1.8M sucrose, 3mM magnesium acetate, 10mM Tris-HCl
567 (pH 8.0)] and centrifuged at 139,800 x g for 2 hours at 4°C. Cellular debris and lysis and sucrose
568 buffers were removed and the pelleted nuclei were resuspended in 500uL PBS. Nuclei were

569 then labeled in a solution of anti-NeuN antibody conjugated to Alexa Fluor 488 (A60, Millipore,
570 1/1000) and 0.1% BSA, rocking for 30 minutes at 4ºC, followed by the addition of DAPI. Nuclei
571 sorting was performed at the Johns Hopkins School of Public Health Flow Cytometry Core with
572 a MoFlo Legacy (Beckman Coulter) using Summit (version 4.3) software. The purity of sorted
573 populations was determined to be >99% based on resorting NeuN+ and NeuN- populations
574 through the same gates.

575 The identity of the NeuN+ and NeuN- populations as neuron-enriched and glia-enriched
576 was confirmed by sequencing nuclear RNA from each population and determining that neuronal
577 and glial biological processes were enriched in genes differentially expressed between the two
578 groups (FDR<0.05; **Figure S1B**). Likewise, cell type marker gene expression patterns also
579 corroborated the neuronal- and glial-enriched identities of NeuN+ and NeuN- samples (**Figure**
580 **S1C**). The estimated proportion of neurons in homogenate DNA methylation data based on
581 deconvolution using differentially methylated sites between NeuN+ and NeuN- samples was
582 highly correlated with the empirical proportion of neurons (**Figure S1D**). Raw sorting data is
583 shown in **Figure S16**.

584 *Nucleic acid extraction and RNA-seq library preparations*

585 RNA was extracted from homogenate and sorted samples using TRIzol LS Reagent (Thermo
586 Fisher Scientific) followed by the RNeasy MinElute Cleanup Kit (Qiagen). Genomic DNA
587 extraction was performed using the DNeasy Blood and Tissue Kit (Qiagen). Bisulfite conversion
588 of 600 ng genomic DNA was performed with the EZ DNA methylation kit (Zymo Research). RNA
589 sequencing libraries were made with the TruSeq RNA Library Prep Kit (Illumina) and the
590 RiboGone Low-Input Ribosomal RNA Removal Kit (Clontech). Library concentrations were

591 measured using a Qubit 2.0 and library fragment sizes were measured using a Caliper Life
592 Sciences LabChip GX. One hundred base-pair paired-end sequencing was run on an Illumina
593 HiSeq 2000.

594 *Whole genome bisulfite library preparations and sequencing*

595 Sequencing libraries were made with Illumina TruSeq DNA Methylation library preparation kits.
596 Lambda (λ) DNA sequence was spiked in at 1% concentration to assess bisulfite conversion
597 efficiency. Library concentrations were measured using a NanoDrop and library fragment sizes
598 were measured using an Agilent Bioanalyzer 2100. Libraries were spiked in with 10% PhiX to
599 improve base calibration calls and subsequently sequenced on an Illumina X-Ten Platform with
600 paired-end reads (2x150bp), targeting 30x coverage and Q30 > 70% read quality.

601 *Data processing/alignment*

602 We sought to align the paired-end reads for each sample to the in-silico bisulfite-treated hg19
603 genome, which we created using the Bismark v0.15.0[37] `bismark_genome_preparation`
604 program. For each library of paired-end reads (one per sample), the following processing was
605 performed (**Figure S17**):

606 · FastQC v0.11.4, to assess read quality, presence of adapter sequence, and
607 overrepresented sequences.

608 · Trimmomatic v0.35[38] to trim low quality and adapter-containing portions of the reads, with
609 the following parameters: `PE -threads 12 -phred33`
610 `ILLUMINACLIP:/Trimmomatic-0.35/adapters/TruSeq3-PE.fa:2:30:10:1`

`LEADING:3 TRAILING:3 SLIDINGWINDOW:4:15 MINLEN:75`. This resulted in three sub-libraries of reads per sample: one paired-end sub-library, and then two single-end sub-libraries where the other corresponding paired read was trimmed to a length below the defined threshold.

- FastQC v0.11.4, on each of the three sub-libraries, to assess the improvement in read quality and adapter content following trimming.
- FLASh v1.2.11[39], to merge the paired-end sub-library reads into longer single-end reads, as reads that overlapped around CpGs and CpHs might bias or at the least double-count the DNAm estimates. Furthermore Bismark[37] could only be run on single- or paired-end reads and not a combination of both. This therefore further split the paired-end sub-library into three sub-libraries: the subset of paired-end reads that were merged into longer single-end reads, and then left and right single-end reads that could not be merged.
- Bismark v0.15.0[37], to align each of the five now-single-end sub-libraries (left-trimmed, right-trimmed, FLASh-merged, FLASh-left-unmerged, and FLASh-right-unmerged) to the bisulfite-converted hg19 genome using bowtie2[40] and the --non-directional argument.
- Resulting alignment (BAM) files across five sub-libraries were merged, sorted, and indexed using samtools v1.3[41] to produce one large/merged BAM file per sample.
- Alignments with evidence of duplication were removed using the MarkDuplicates program in Picard tools v1.141, which systematically appeared to be localized to low complexity DNA sequence near centromeres.
- The Bismark[37] `bismark_methylation_extractor` program was run on each post-duplicate-removed BAM file per sample to extract CpG and CpH DNAm levels.

633 We additionally aligned reads from each sample to the PhiX and Lambda (λ) genomes to
634 compute quality control metrics related to sequencing and bisulfite conversion quality. The
635 average percentage of reads mapping back to the λ genome was 1.32% and the average
636 bisulfite conversion efficiency was 98.64%. The average bisulfite conversion efficiency was not
637 associated (p>0.05) with cell type, age, cell type (adjusting for age), age (adjusting for cell type),
638 and the interaction of them in the NeuN- (glia) and NeuN+ (neuron) samples as well as for age
639 in the homogenate samples. The genome coverage decreased from an initial average of 43x to
640 10x across the processing stages as shown in **Figure S18 (coverage)**. For each of the
641 processing stages, there was no significant difference between cell types (adjusting for age),
642 age (adjusting for cell type) as well as the interaction between age and cell type (p
643 Bonferroni>0.05). The genome coverage was extracted from the `FASTQC` reports and by using
644 `bamcount` (https://github.com/BenLangmead/bamcount) v0.2.6.

645 *Identifying methylation features*

646 We identified PMDs, UMRs and LMRs using the bioconductor package MethylSeekR (version
647 1.20.0). We obtained coverage information from the cleaned set of ~18 million CpGs by
648 extracting coverage and methylation using the `getCoverage()` function from the bsseq
649 bioconductor package[42] v1.10.0. PMDs were called using `segmentPMDs()` and were visually
650 inspected using `plotPMDSegmentation()`. To create a more stringent cutoff for PMDs, we
651 filtered PMDs to those longer than 100 Kbp. We calculated the FDRs using
652 `calculateFDRs()`, while masking the >100 Kbp PMDs, setting the m parameter to 0.5 and
653 the FDR cutoff to 10. PMDs were further filtered to exclude overlaps with the UCSC "gap"
654 database table from hg19 except for the gaps labeled heterochromatin. We calculated UMRs

655 and LMRs using `segmentUMRsLMRs()`. DMVs were defined as UMRs in which pmeth was less
656 than or equal to 0.15 and the width was greater than or equal to 5 Kbp.

657 *Identifying CpG differentially methylated regions (DMRs)*

658 Using the bsseq[42] Bioconductor package v1.10.0 we loaded the Bismark[37] report files and
659 filtered the CpG data to keep only the bases where all samples had a minimum coverage of 3
660 (18,664,892 number passed the filter). We smoothed the methylation values of the remaining
661 CpGs using the `BSmooth()` function from bsseq with the `parallelBy="sample"` option. To
662 identify the age and cell type DMRs we used a model that adjusted for both covariates while for
663 the interaction model we included an additional interaction covariate. We identified the DMRs
664 using the bumphunter[43] Bioconductor package v1.14.0 using the `maxGap=1000`, `B=250`,
665 `nullMethod="permutation"`, `smooth=FALSE` options, which tends to be conservative in
666 DMR identification[43]. For the `cutoff` option we used 0.1 for the cell type DMRs adjusting for
667 age, 0.005 for the age DMRs adjusting for cell type, and 0.009 for the age and cell type
668 interaction DMRs. These first two parameter cutoffs correspond to 10% minimum DNAm
669 differences between neurons and glia and 5% change in DNAm per decade of life across cell
670 types, and were chosen based on functionally-relevant change in DNAm. The cutoff for the
671 interaction model (cdDMRs) was based on selecting the equivalent percentile of change from
672 the overall age model (86th percentile) - this percentile-based cutoff was in line with
673 recommendations for selecting cutoffs for statistical models with less clear biological
674 interpretations[43]. We used a family wise error rate (FWER) threshold of 5% to determine the
675 DMRs: `fwer` output from the `bumphunter()` function. A small subset of DMRs involved a
676 single CpG, which arises from having a more significant area (length times effect size) than any

677 DMRs identified in null permuted data. All DMRs showed less than 10% median percent
678 absolute bias to technical and biological covariates as shown in **Figure S19 (sensitivity)**.

679 *cdDMR processing*

680 For the "interaction" DMRs with FWER<5% (cdDMRs) we extracted the methylation values from
681 the glial and neuronal samples using bsseq[42] v1.13.9 and then computed a mean methylation
682 value per DMR for each cell type. We also calculated the mean interaction coefficient for each
683 DMR across all the cytosines in the DMR by cell type. Using the mean coefficients by cell type
684 we clustered the interaction DMRs using the `kmeans()` function with `centers=6`,
685 `nstart=100` options. We chose `centers=6` based on biological interpretability of the results
686 and because k=6 results in an optimal AIC for clusters computed with mean centered and
687 scaled data. For each cytosine in the cdDMRs we calculated the t-statistic and coefficient for
688 age explaining differences in methylation adjusted for cell type: `~ age + cell type`. For
689 each DMR we computed the mean age coefficient by cell type and then calculated the median
690 absolute coefficient across all cdDMRs. The neuronal / glia ratio is 1.5 for such median absolute
691 age effects across the cdDMRs.

692 *Comparing homogenate vs. cell type-specific WGBS*

693 We first filtered CpGs to those with coverage in all 55 postnatal samples. For homogenate
694 samples, we used `lmFit()` and `ebayes()` from the limma[44] Bioconductor package v3.34.5 to
695 assess age-associated changes to DNAm levels with the linear model `~ Age`. For the cell
696 type-specific samples, we used a linear model `~ Age * Cell Type` to assess cell type,
697 overall age, and age in a cell type changes to DNAm levels. We subset CpGs to those that were

698 significantly differentially methylated by age in homogenate samples ($p<1x10^{-4}$) and plotted the
699 coefficients for each CpG in **Figure S2A-D**. The relationship between each variable was
700 quantified using Fisher's exact test.

701 *Roadmap Epigenome enrichments*

702 We computed the relative enrichments of different genomic regions using Epigenome Roadmap
703 data[12] by computing the proportion of bases in each of the 15 ChromHMM states for each of the
704 cells and tissues provided by the Consortium. We compared the proportion of bases in each
705 state within each candidate region set to the overall genome and computed the corresponding
706 log2 enrichments between the regions and this genomic background. We compared DMR and
707 mCpG-based methylation feature regions to all profiled cell types in the Consortium for these
708 analyses.

709 *Assessing the contribution of neuronal subtypes*

710 The percent of neuronal subtype-specific bases were calculated by reducing the total
711 subtype-specific CpG-DMRs from Luo *et al*.[14], reducing the bases in each group of cdDMRs and
712 calculating the percent of cdDMR bases that intersected the merged subtype-specific CpG-DMR
713 bases.

714 *Visualizing DMRs*

715 Plots for the DMRs were made using bsseq[42] v1.14.0, EnsDb.Hsapiens.v75 v2.99.0, and
716 RColorBrewer v1.1-2. Genes within 20 kb of a DMR were retained for the plots. Genes and

717 exons were included using the `annoTrack` argument and we used extend=`2000` for making the
718 plots.

719 *CpH processing*

720 Using Bismark v0.16.3[37] we created report files using the methylation extractor program with the
721 `CX_context` and `split_by_chromosome` options for the hg19 human genome in order to
722 extract the methylation values for the CpHs. Then for each chromosome, using the bsseq[42]
723 Bioconductor package v1.10.0 we loaded the Bismark[37] report files and added the c_context
724 and trinucleotide_context information from Bismark using custom R code based on the bsseq
725 internal code that uses the data.table package v1.10.4. After combining the results for each
726 chromosome, we filtered the CpHs to keep only those where all samples had a minimum
727 coverage of 5 (58,109,566 number passed the filter).

728 *Lister, et al. (2013) data processing*

729 We downloaded the WGBS data from Lister *et al.* data[1] with SRA accession SRP026048. We
730 then processed and aligned the data following the same steps we used for our data. Using
731 bsseq[42] as in the *CpH processing* section, we extracted the methylation values from the
732 Bismark[37] report files and added the `c_context` and `trinucleotide_context` information
733 per chromosome. We then merged the results for all the chromosomes retaining only the CpG
734 and CpH positions we observed with a minimum coverage of 3 and 5 in our data, respectively.
735 To assess the replication of our cell type DMR results we computed mean methylation
736 differences across the CpG positions comparing neuron and non-neuron samples in the Lister *et*
737 *al.* data[1] using the `rowttests()` function from the genefilter package version 1.56.0. We then

computed the mean difference for each of the DMRs and compared this mean difference against the DMR mean methylation difference derived from our data to derive the concordance and correlation between them. To assess the replication of our age DMR results we modeled age as a continuous variable and calculated the mean methylation difference per year for every CpG contained in the age DMRs using `lmFit()` function from limma. Finally, we compared the mean methylation difference in the Lister *et al.* data[1] against the observed mean methylation difference for the age DMRs we derived.

Homogenate data processing

We processed the prenatal and postnatal homogenate brain samples using the same procedure described in the *Data processing/alignment* section to produce Bismark[37] report files. Then using bsseq[42] we extracted the methylation values for the CpG positions observed in our postnatal samples in order to make them comparable to each other.

Identification of differentially methylated positions

With the set of CpGs and CpHs with a minimum coverage 3 and 5 in all samples, respectively, and the same models for identifying the DMRs, we identified the differentially methylated positions (DMPs), keeping the CpGs and CpHs separate. For the CpHs we further filtered to keep only those where at least 5 samples had a methylation value greater than 0 (40,818,742, 70.2%). We used the limma Bioconductor package v3.30.13 for determining the DMPs by running functions `lmFit()` and `eBayes()` with default parameters and FDR<5%.

757 *Enrichments for HARs and enhancers*

758 We calculated the enrichment of genomic segments overlapping cdDMRs and human
759 accelerated regions (HARs) and enhancers[15] using Fisher's exact test. We calculated the
760 overlap of methylation features (DMRs, mCpH, expression-associated cytosines) and HARs or
761 enhancers with the entire set of CpG clusters used to identify the DMRs as background. We
762 corrected for multiple testing using the false discovery rate (FDR).

763 *Stratified linkage disequilibrium score regression*

764 GWAS summary statistics for 30 phenotypes (described in Anttila et al. and Rizzardi et
765 al.)[20,21] were downloaded from the sources listed in Table S6. We used LDSC (LD SCore) v1.0.0
766 to estimate the proportion of heritability captured in 16 sets of genomic DNAm features for each
767 GWAS phenotype, including the DMRs and LMRs defined above in this work, non-differentially
768 methylated CpG clusters (called above before the DMR analysis, excluding DMR sequence),
769 central nervous system annotations included in the LDSC package (referred as CNS (LDSC)),
770 and regions annotated as putatively regulatory in human brain using chromHMM (i.e., the union
771 of regions annotated as "Bivalent Enhancer", "Bivalent/Poised TSS", "Genic enhancers",
772 "Flanking Active TSS", "Active TSS", "Strong transcription", and "Enhancers" in the following
773 tracks accessed using the AnnotationHub Bioconductor package (v2.14.5)[45]: AH46920,
774 AH46921, AH46922, AH46923, AH46924, AH46925, AH46926, AH46927, AH46934, and
775 AH46935).

776 We first converted the GWAS summary statistics into the `.sumstats` format using
777 `munge_sumstats.py` and keeping only HapMap 3 SNPs (downloaded from
778 https://data.broadinstitute.org/alkesgroup/LDSCORE/w_hm3.snplist.bz2) as described in the

779 Partitioned Heritability LDSC tutorial. We made `.annot` files for each custom feature set based
780 on the list of SNPs in the CNS cell type annotations provided in the LDSC package and
781 estimated partitioned LD scores for each feature using 1000 Genomes plink files (downloaded
782 from https://data.broadinstitute.org/alkesgroup/LDSCORE/1000G_Phase3_plinkfiles.tgz) using
783 `ldsc.py`. We finally estimated the partitioned heritability for each feature-phenotype
784 combination by adding each feature individually to the "baseline model" including 53 baseline
785 annotations described in Finucane et al.[22]

786 *Enrichments for genes associated with brain disorders*

787 We calculated the enrichment of genes overlapping different methylation features in gene sets
788 described by Birnbaum *et al*.[24] We measured what fraction of the genes in each set overlapped
789 methylation features (ie, DMRs, mCpH, and expression-associated cytosines) with Fisher's
790 exact test using all expressed genes with Entrez IDs as background. We corrected for testing
791 multiple disorder gene sets using the false discovery rate (FDR).

792 *RNA-seq data processing*

793 Raw sequencing reads were mapped to the hg19/GRCh37 human reference genome with
794 splice-aware aligner HISAT2 v2.0.4[46]. Feature-level quantification based on GENCODE release
795 25 (GRCh38.p7) annotation on hg19 coordinates was run on aligned reads using featureCounts
796 (subread v1.5.0-p3)[47]. Using custom R code we processed the different feature counts and
797 created RangedSummarizedExperiment objects using the SummarizedExperiment
798 Bioconductor package v1.4.0.

799 *Percent spliced in (PSI) calculation*

800 We calculated the percent spliced in using the SGSeq[48] Bioconductor package v1.12.0 and the
801 Gencode v25 annotation for the GRCh37 human reference genome
802 (ftp.sanger.ac.uk/pub/gencode/Gencode_human/release_25/GRCh37_mapping/gencode.v25lift
803 37.annotation.gtf.gz) from the BAM files generated by HISAT2. We used default arguments
804 except for the function `analyzeVariants()` where we used a `min_denominator=10`.

805 *Differential expression between cell types*

806 We combined the gene counts for the polyA+ and RiboZero sequencing protocols for the
807 cell-sorted RNA-seq data: 3 NeuN+ and 3 NeuN- samples for a total of 12 RNA-seq sequencing
808 runs. We calculated the library size normalization factors using `calcNormFactors()` from
809 edgeR[49] (v3.22.3) and identified the differentially expressed genes using `voom()`, `lmFit()` and
810 `eBayes()` from limma[44,50]. We repeated this procedure for the exon counts.

811 *Gene ontology analyses*

812 Gene ontology enrichment analyses were performed using clusterProfiler[51] v3.6.0 using the
813 options `pAdjustMethod="BH"`, `pvalueCutoff=0.1`, and `qvalueCutoff=0.05` on the
814 Entrez IDs for each expression feature for the BP, CC and MF GO ontologies. Only cytosines or
815 DMRs overlapping genes were included.

816 *Methylation vs expression associations*

With the sorted RNA-seq data, we computed the average gene expression per age group (infant, child, teen) and cell type (six groups), and correlated these values to average DNAm levels in the same groups in both the CpG and CpH contexts at the gene promoter and body, exon (500bp window), and splice junction (50bp into each intron) levels. With the RangedSummarizedExperiment objects with the RNA-seq polyA homogenate data and the bsseq objects with the CpG and CpH data we determined which CpG and CpH positions explained changes in expression (RPKM) at the gene or exon level as well as in percent spliced in (PSI). We retained only the expression and PSI data from the postnatal samples and matched them by brain identifier to the neuronal methylation data with a final sample size of 22. We filtered lowly expressed features using the `expression_cutoff()` function from the jaffelab package v0.99.18: mean RPKM>0.22 mean for genes, 0.26 for exons. For genes and exons we transformed the expression values to log2(RPKM + 1) and extracted the raw PSI values. Using MatrixEQTL[52] v2.2 (GitHub b9a9f01 patch) we then identified the methylation quantitative trait loci (QTL) for the CpG and CpH methylation data separately using the function `Matrix_eQTL_main()` function with options `pvOutputThreshold=0`, `pvOutputThreshold.cis=5e-4`, `useModel=modelLINEAR`, `cisDist=1000`. We identified marginal CpG associations near CpH associations by running MatrixEQTL again for the CpG in a +- 1kb window around the CpH positions with an association with expression at FDR <5% for each expression feature type using the same parameters as above except for `pvOutputThreshold.cis=0.01`. We filtered the associations to retain only those having at least 11 samples with non-zero methylation and 11 samples with non-one methylation values to remove extreme cases. We further restricted the results to protein coding genes and dropped any with infinite t-statistics. To assess whether age confounds the relationship between methylation and expression, we used a multiple linear regression model adjusting for age and

841 checked if the methylation coefficient was still FDR<5%. Venn diagrams in **Figure 3** were made
842 with the VennDiagram package v1.6.18. For the gene and PSI associations we used the gene
843 ID to check if it was present in the 3,473 differentially expressed genes from the sorted RNA-seq
844 data (described above) with higher expression in neurons and the top 5,000 DE genes with
845 higher expression in glia at FDR<5%; similarly we did so for exons and the top 5,000 DE exons
846 (FDR<5%) with higher expression in each cell type. The LIBD WBGS Expression explorer at
847 https://jhubiostatistics.shinyapps.io/wgbsExprs/ was made using the bsseq[42] v1.14.0, DT v0.4,
848 SGSeq[48] v1.12.0 and shiny v1.0.5 R packages.

849 *Global autocorrelation*

850 Using CpG and CpH positions with a minimum coverage of 3 and 5 respectively for all samples
851 we calculated the autocorrelation for the methylation levels for the CpGs, the CpHs, the CpHs
852 with a CHG trinucleotide context, or the CpHs with a CHH trinucleotide context. For each of the
853 sets, we grouped the positions using derfinder v1.12.0 into groups by a maximum distance of 1
854 kb. Only those groups with at least 5 Cs were further considered. For each sample we then
855 calculated the autocorrelation using the `acf()` function with `lag.max=4` in parallel for each
856 chromosome using BiocParallel v1.12.0. For each cluster of cytosines we calculated the mean
857 across the neuronal (NeuN+) and the glia (NeuN-) samples at each autocorrelation lag. After
858 combining and tidying the results, we visualized the global auto correlation using ggplot2 v2.2.1.
859 We repeated this same analysis for the Lister *et al.* data[1].

860 *Autocorrelation within DMRs*

861 Similar to the global autocorrelation, we extracted the methylation values at CpGs with a
862 minimum coverage of 3 and the CpHs with a minimum coverage of 5 that were within each of
863 the sets of DMRs (age, cell type or interaction). We then computed the autocorrelation for DMRs
864 with a least 5 different cytosines using the acf() function with a lag.max=4 and calculated the
865 mean auto-correlation among the neuronal and glial samples. The lag is proportional to the
866 genomic distance as shown in **Figure S20 (lag and distance)**.

867 **Table 1: Summary of methylation-expression associations**. Mean values are shown for the

868 number of samples with β>0, β<1, and expression change variables (either ΔPSI or

869 Δlog2(RPKM + 1) for genes and exons). Columns from "Age Confounded" are proportions. See

870 **Table S10** for a full description of the variables.

Feature	Meth. Type	Direction	N	N Unique C	N Unique Features	Mean N Meth>0	Mean N Meth<1	Mean Expr Change	Prop. Age Confounded FDR >=5%	Prop. In Promoter	Prop. In Gene Body	Prop. In Gene Flanking	Prop. CHG	Prop. CHH	Prop. DE Glia	Prop. DE Neuron	Prop No Diff
gene	CpG	down	18458	18353	2074	21.9	21.9	1.39	0.0932	0.0671	0.966	0.906	0	0	0.126	0.329	0.546
		up	5217	5021	1743	21.8	21.8	1.69	0.0845	0.0571	0.979	0.92	0	0	0.304	0.193	0.503
	CpH	down	25812	25712	1611	21.1	21.1	1.4	0.115	0.0161	0.519	0.75	0.22	0.781	0.0912	0.413	0.496
		up	3842	3840	846	20.1	20.1	1.66	0.2	0.0219	0.532	0.807	0.26	0.744	0.123	0.27	0.607
exon	CpG	down	9505	4536	4168	21.9	21.9	1.23	0.104	0.19	0.934	0.991	0	0	0.0097	0.0256	0.965
		up	1328	638	687	21	21	1.93	0.191	0.175	0.928	0.988	0	0	0.0369	0.0136	0.95
	CpH	down	7874	4082	3458	21.1	21.1	1.72	0.074	0.0328	0.437	0.927	0.19	0.814	0.0086	0.0451	0.946
		up	1288	733	962	18.7	18.7	1.94	0.154	0.0435	0.481	0.918	0.28	0.722	0.0031	0.0311	0.966
psi	CpG	down	4286	2477	1315	21.7	21.7	0.124	0.0272	0.0434	0.994	0.936	0	0	0.242	0.212	0.547
		up	5782	3915	1646	21.8	21.8	0.121	0.0195	0.0398	0.991	0.919	0	0	0.261	0.222	0.517
	CpH	down	1296	945	489	16.8	16.8	0.447	0.0201	0.0274	0.537	0.676	0.36	0.644	0.187	0.286	0.526
		up	875	536	391	16.5	16.5	0.169	0.032	0.0279	0.559	0.775	0.36	0.637	0.194	0.33	0.477

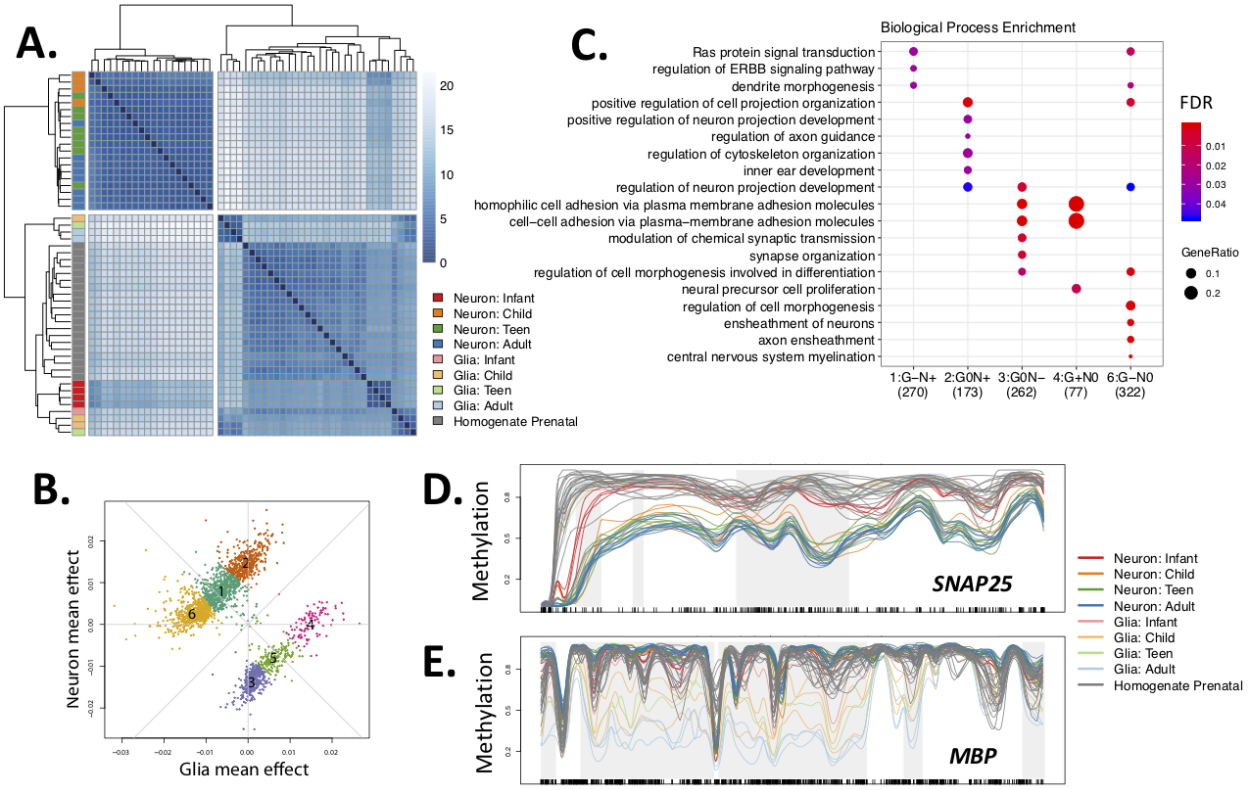

Figure 1: Regional cell type-specific developmental mCpG trajectories. (A) Euclidean distances between samples within cdDMRs shows that older neuronal samples cluster separately from infant neuronal samples, glia regardless of age, and bulk prenatal cortex. **(B)** Decomposing cdDMRs patterns into 6 clusters using *k-means* based on glia and neuron mean mCpG changes per year of life. **(C)** The top five most enriched gene ontology terms for each of the six groups in **(B)** highlights diverse biological processes amongst the groups. No terms were enriched for Group 5. **(D)** Example Group 3 cdDMR within *SNAP25.* **(E)** Example Group 6 cdDMR within *MBP.* Gray shading indicates the boundaries of the cdDMR, and black tick marks on the x-axis indicate the position of CpGs. Key: Neuron (NeuN+); Glia (NeuN-); Infant (0-1 years); Child (1-10 years), Teen (11-17 years) and Adult (18+ years).

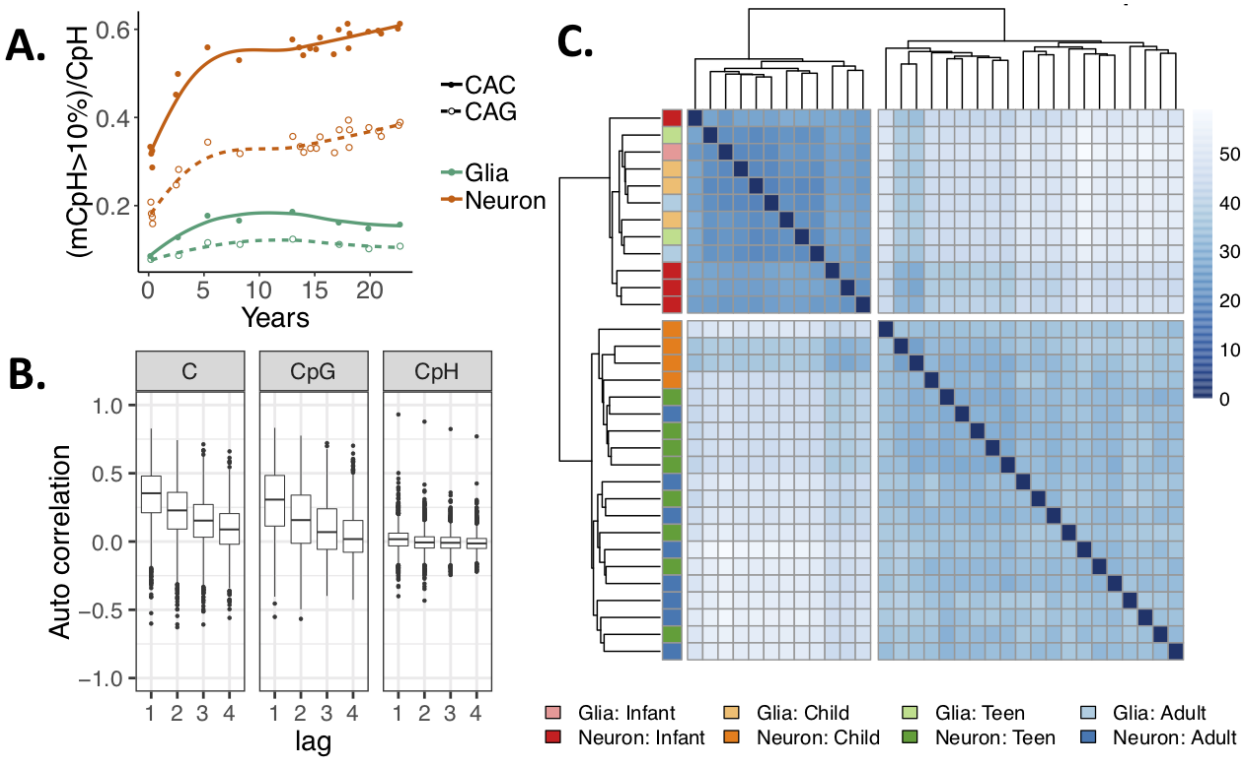

Figure 2: CpH methylation patterns across brain development. (A) The proportion of CAC and CAG sites that are greater than 10% methylated in neurons and non-neurons (glia) across brain development. **(B)** Autocorrelation levels for different cytosine contexts in neurons. Autocorrelation levels were similar for mCpG and all cytosines, with uncorrelated levels in the CpH context. **(C)** Euclidean distances between samples based on mCpH within cdDMRs again cluster infant neurons dark red) with glia of all ages (light colors) rather than with older neurons.

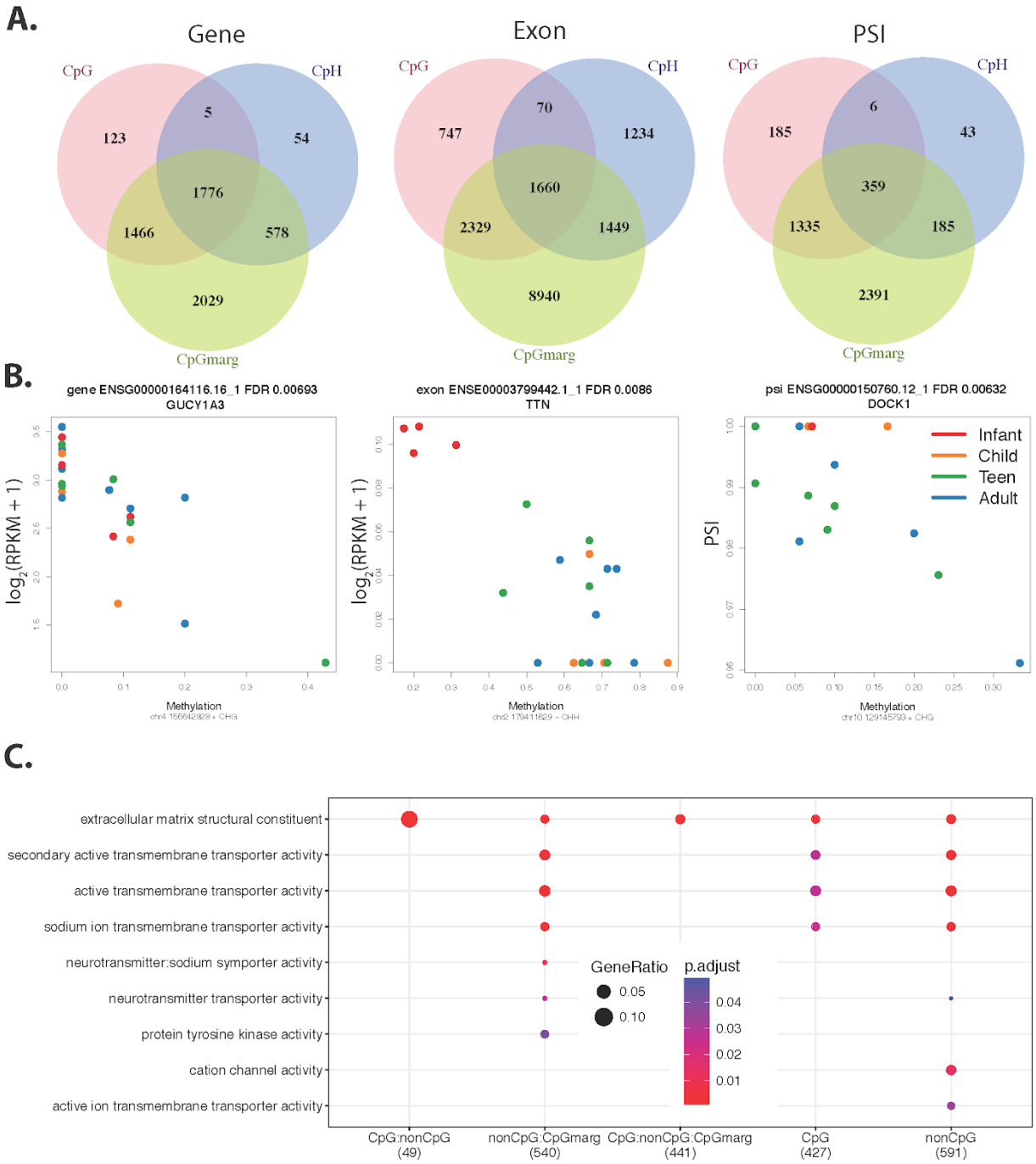

Figure 3: Methylation associations with expression. **(A)** Venn diagrams of the methylation associations by unique feature for the gene, exon and PSI. The sets are determined by if the association is FDR<5% genome-wide for CpG and CpH or if it is a CpG marginally significant within +/- 1 kb window of a CpH association. **(B)** Example associations between methylation

891 and expression at the gene level colored by age: red - infant, orange - child, green - teen, blue -
892 adult. *GUCY1A3* contains one of the top CpH differentially expressed between neurons and glia.
893 Expression of an exon of *TTN*, an autism-associated gene, is negatively associated with mCpH.
894 *DOCK1* PSI of an alternative end site is negatively associated with mCpH. **(C)** Enriched
895 molecular function ontology terms for methylation-associated exons by the venn diagram groups
896 from (A).

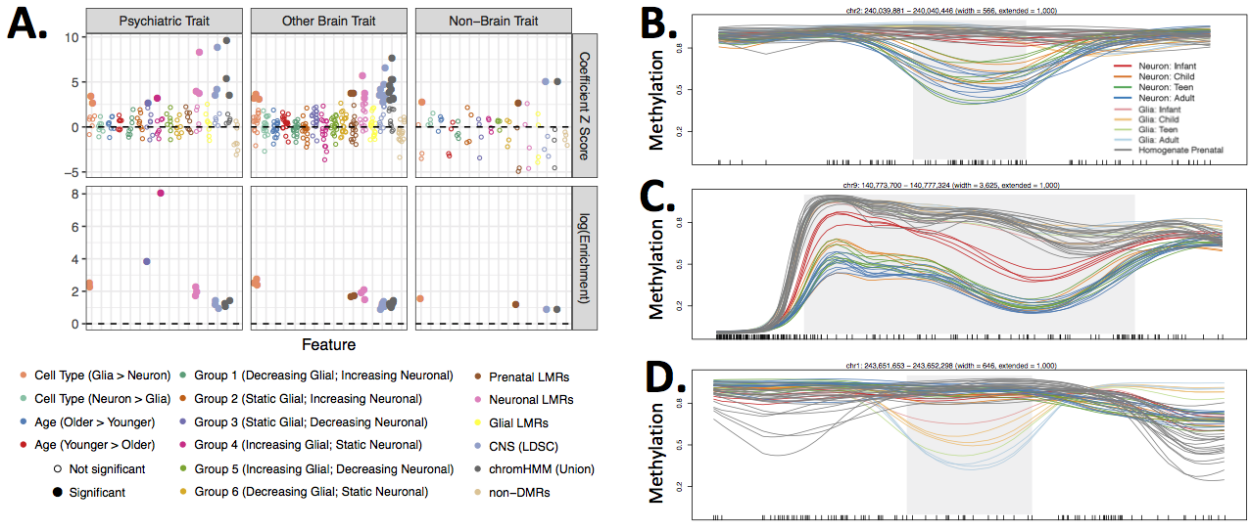

Figure 4: DNAm patterns and brain trait heritability. **(A)** Results assessing enrichment for heritability of 30 phenotypes within 16 groups of DNAm features using Stratified Linkage Disequilibrium Score Regression (SLDSR). Each dot represents results for a single phenotype:DNAm feature pair. The color indicates the DNAm feature, and the phenotypes are stratified by column into psychiatric phenotypes, other brain-related phenotypes (ie, neurological or behavioral-cognitive), or non-brain-related traits. The upper row shows the coefficient Z score for each tested phenotype:DNAm pair, or the amount of additional heritability explained by the DNAm feature over 53 baseline features in the SLDSR model. The lower row shows the enrichment score, or the proportion of heritability attributed to the feature divided by the proportion of SNPs in the feature. For clarity enrichment scores of only the significant feature-trait combination are depicted. Filled in circles indicate significantly enriched heritability for a phenotype in a feature (coefficient p-value corrected using Holms method≤0.05). **(B)** A cdDMR overlapping *HDAC4*, a gene associated with autism spectrum disorder (ASD), shows the Group 3 pattern of decreasing neuronal and static glial DNAm. **(C)** A cdDMR overlapping *CACNA1B*, a gene associated with ASD, shows the Group 5 pattern of decreasing neuronal and increasing glial DNAm. **(D)** A cdDMR overlapping *AKT3*, a gene associated with schizophrenia,

913 shows the Group 6 pattern of decreasing glial and static neuronal DNAm. Gray shading
914 indicates the boundaries of the cdDMR, and black tick marks on the x-axis indicate the position
915 of CpGs.

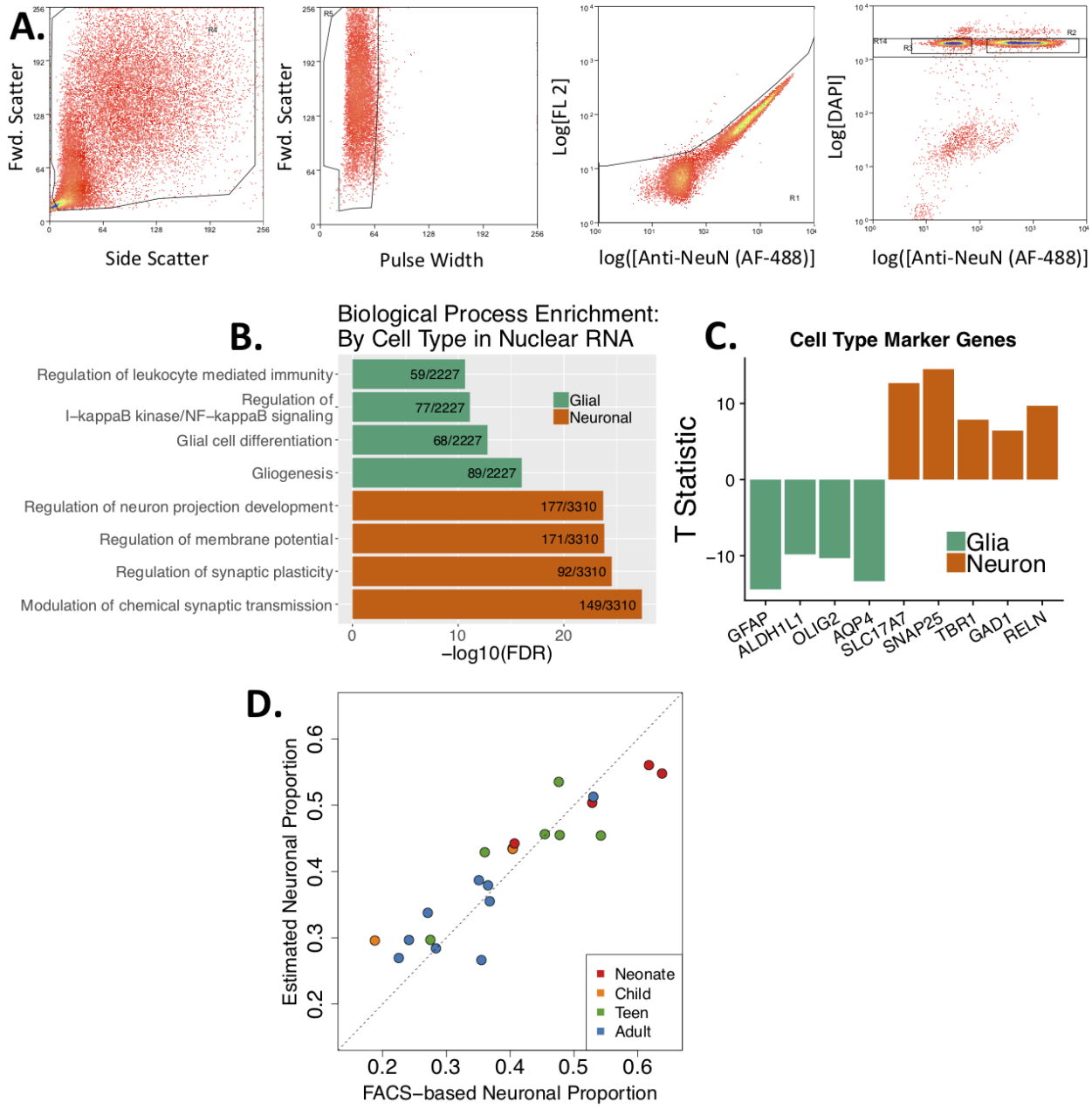

Figure S1: Confirmation of neuronal- and glial-enriched identity of NeuN+ and NeuN- samples. (A) Representative gating strategy from fluorescence-activated nuclear sorting by NeuN antibody. Debris is first reduced by selecting events based on forward scatter and side scatter, then aggregates are reduced by measuring pulse width. Autofluorescent events are discarded by measuring true Alexa fluor-488 signal compared to signal in the FL2 channel.

921 Finally, singlets are determined by DAPI staining, and Alexa fluor-488 positive and negative
922 events are collected. **(B)** Top biological processes enriched in genes significantly differentially
923 expressed in nuclear RNA from NeuN+ (labeled “Neurons”) and NeuN- (labeled “Glia”) at
924 FDR<0.05. **(C)** T statistics for marker genes for neuronal and non-neuronal identity show that
925 the genes are differentially expressed in NeuN+ and NeuN- nuclear RNA (FDR<0.05). **(D)** The
926 estimated proportion of neurons in homogenate WGBS samples based on statistical
927 deconvolution using differentially methylated cytosines between NeuN+ and NeuN- samples is
928 highly correlated with the empirically-derived proportion of NeuN+ events.

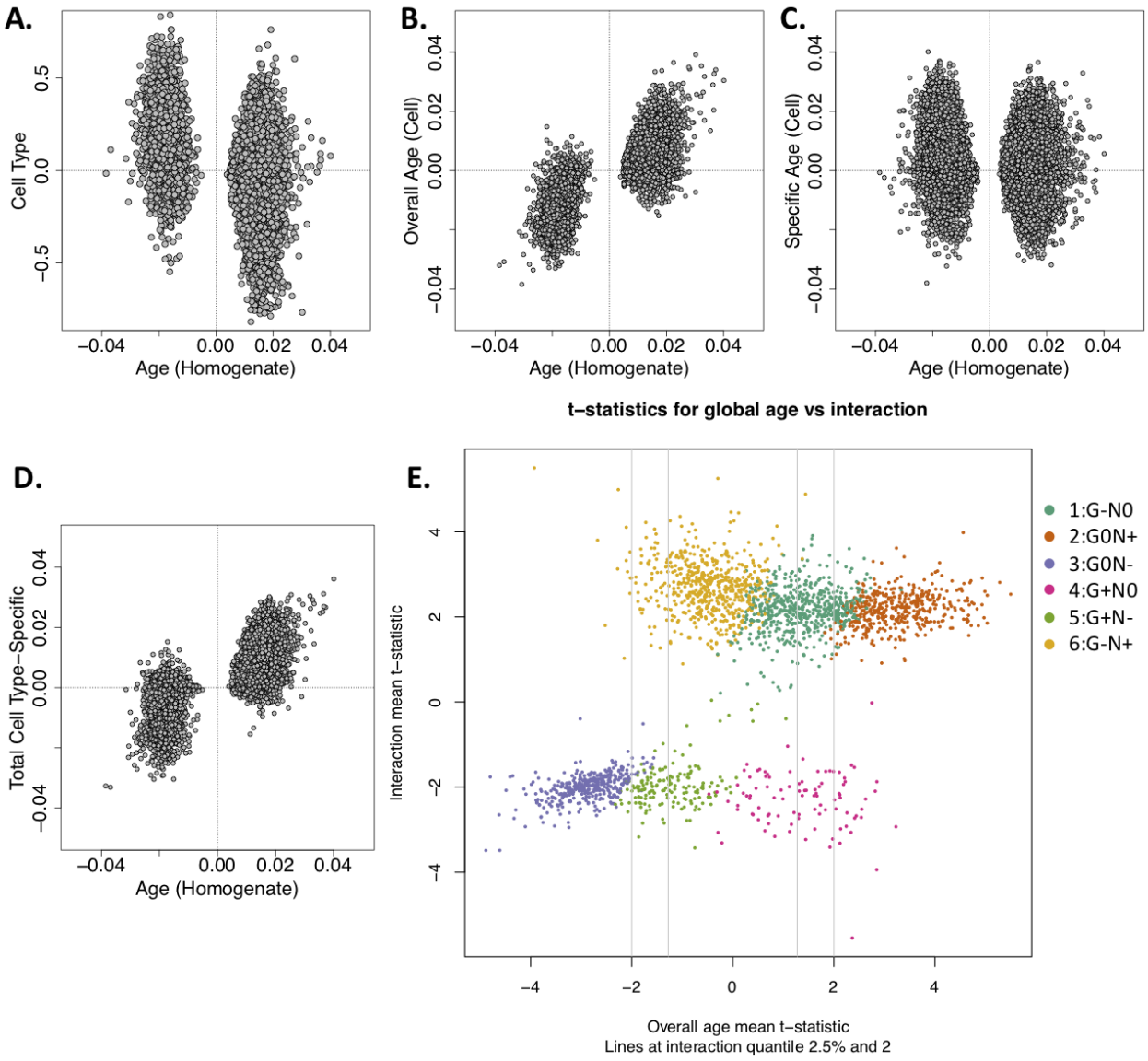

929 **Figure S2: Detecting developmental changes in homogenate vs. cell type-specific DNAm**
930 **data. (A)** Developmental age effect coefficients of individual CpGs as measured in homogenate
931 samples compared against cell type effect coefficients in cell type-specific samples after
932 adjusting for age. **(B)** Developmental age effect coefficients of individual CpGs as measured in
933 homogenate samples compared against the developmental effect adjusting for cell type in cell
934 type-specific samples. **(C)** Developmental age effect coefficients as measured in homogenate
935 samples compared against the cumulative age and cell type interaction effect coefficients in cell

936 type-specific samples at the CpG level. **(D)** Developmental age effect coefficients as measured
937 in homogenate samples compared against the estimated cell type-specific age effects for cell
938 type-specific samples at the CpG level. **(E)** Overall age mean t-statistic for the cdDMRs (x-axis)
939 against the mean interaction t-statistic (y-axis) with the 2.5% quantile from the y-axis shown on
940 the x-axis. Colors are the same as those from **Figure 1B**: teal=Group 1 (decreasing glial
941 methylation, increasing neuronal methylation), orange=Group 2 (static glial methylation,
942 increasing neuronal methylation), purple=Group 3 (static glial methylation, decreasing neuronal
943 methylation), pink=Group 4 (increasing glial methylation, static neuronal methylation),
944 green=Group 5 (increasing glial methylation, decreasing neuronal methylation), gold=Group 6
945 (decreasing glial methylation, static neuronal methylation).

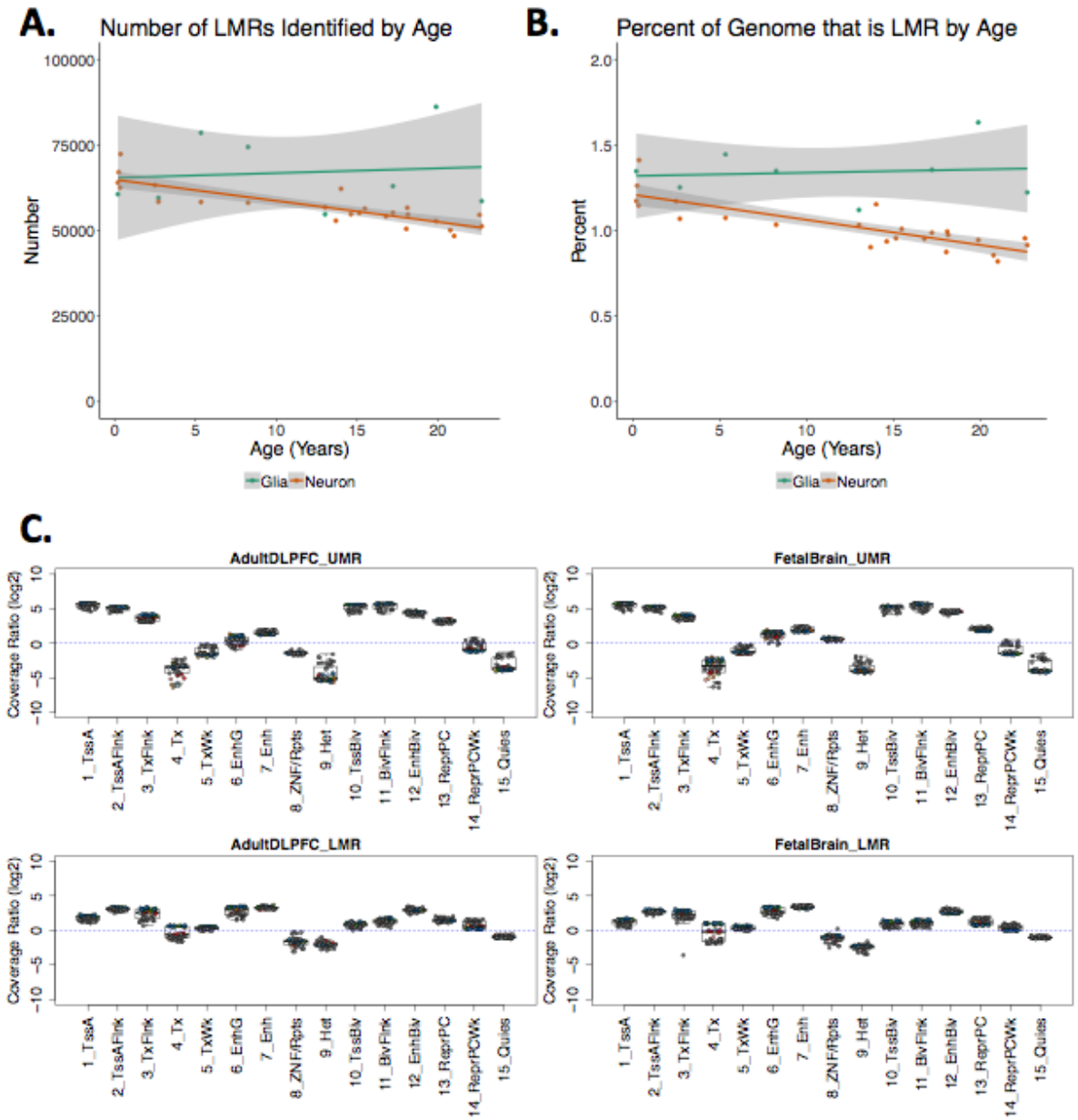

Figure S3: Unmethylated Regions (UMRs) and Low-methylated regions (LMRs). (A) Number of LMRs and **(B) p**ercent of the genome covered by LMRs by age stratified by cell type. Shading indicates the standard error of the linear model. **(C)** Roadmap Epigenomics Consortium predicted chromatin-enriched states for LMRs and UMRs as defined in adult DPLFC and fetal brain. log2(Coverage Ratio) represents the enrichment of the proportion of bases within LMRs or UMRs in a chromatin state compared to the rest of the genome.

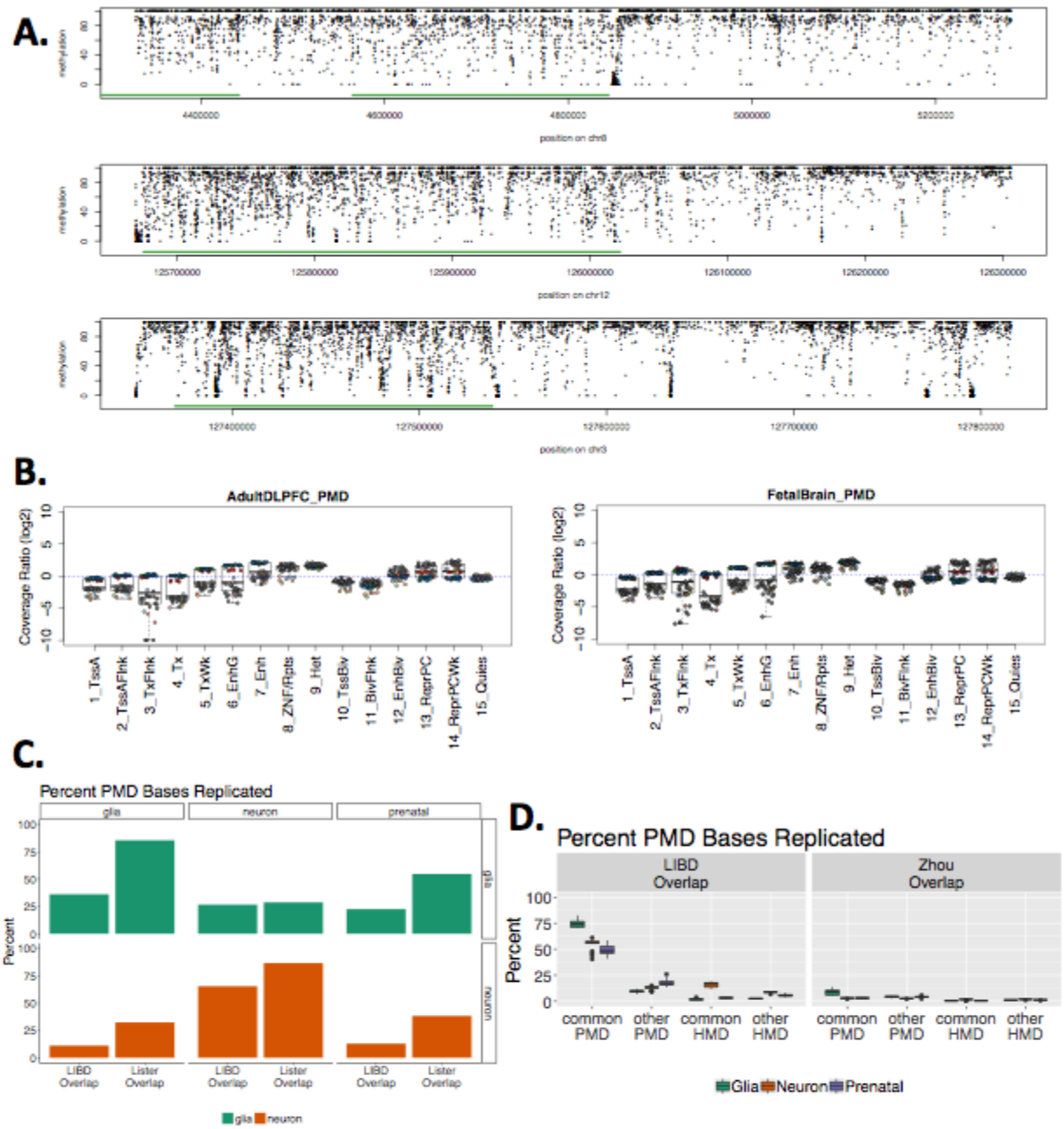

Figure S4: Partially methylated domains (PMDs). (A) Example PMDs on chromosomes 8, 12, and 3. PMDs are highlighted in green. **(B)** Roadmap Epigenomics Consortium chromatin state enrichment for PMDs. log2(Coverage Ratio) represents the enrichment of the proportion of bases within PMDs in a state compared to the rest of the genome. **(C)** Percent of PMD

956 base-pairs that are replicated in the Lister *et al.* (2013) FANS samples[1]. Rows represent Lister
957 *et al.* (2013) glia and neurons, and columns represent the glia, neurons and prenatal samples
958 from this paper (LIBD). Each bar represents the percent of PMD bases shared between that
959 quadrant's cell types, using either total LIBD or total Lister PMD bases as the denominator. **(D)**
960 Percent of PMD base pairs per sample that are replicated in either common or unique PMDs
961 and high methylated domains (HMDs) identified in Zhou *et al.*[13] Samples are colored based on
962 whether the sample was postnatal neuron, postnatal glia, or bulk prenatal cortex.

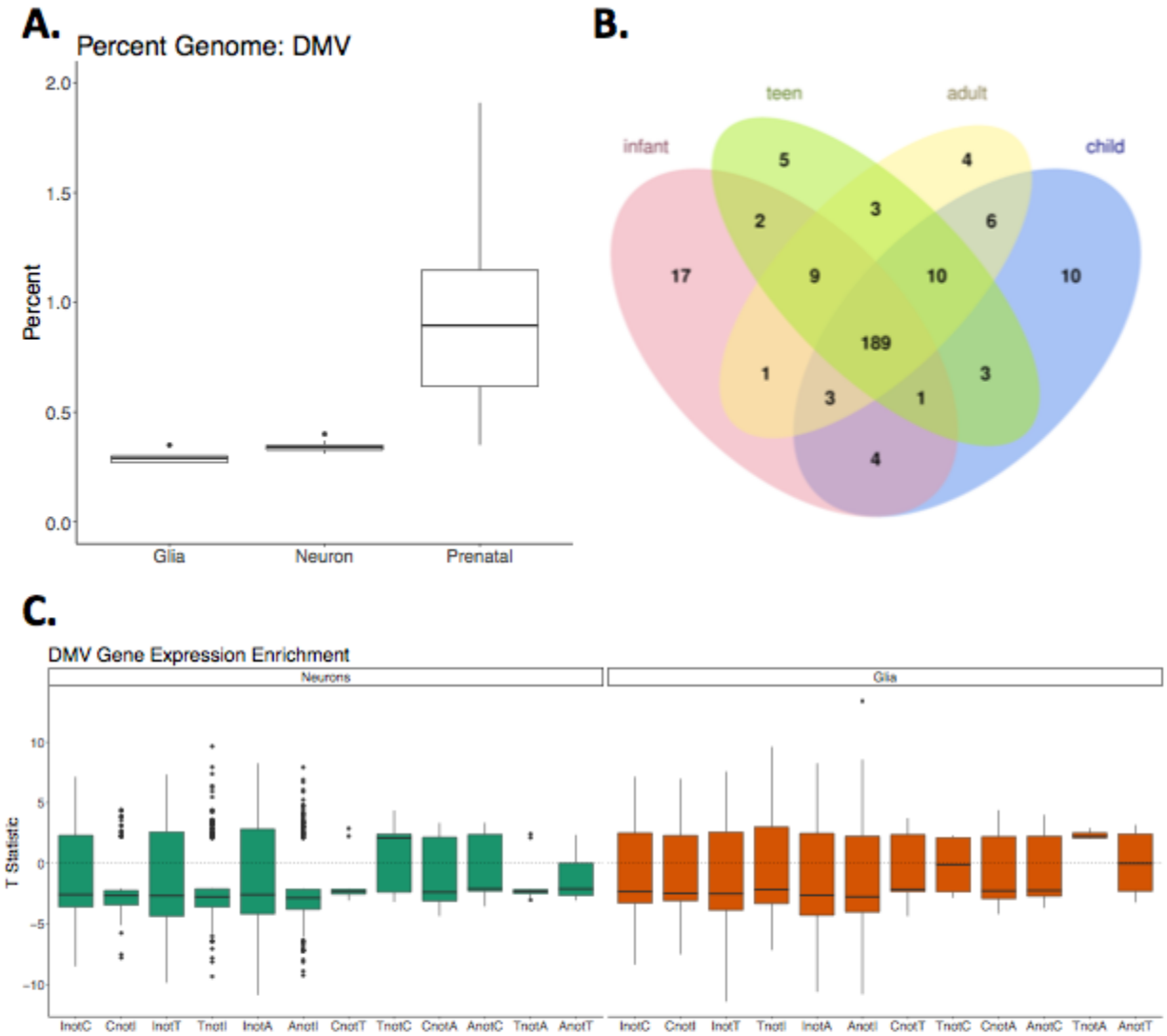

963 **Figure S5: DNA methylation valleys (DMVs). (A)** Percent of the genome covered by DMVs in
964 postnatal glia and neurons and bulk prenatal cortex. **(B)** Overlap of transcription factor (TF)
965 genes within DMVs by age in neurons. **(C)** Expression enrichment between age groups in TF
966 genes excluded from DMVs in one group but not the other in neurons and glia. A negative
967 T-statistic signifies greater expression in the age group in which the gene is not in a DMV.
968 I=Infant (0-1 years); C=Child (1-10 years), T=Teen (11-17 years) and A=Adult (18+ years).

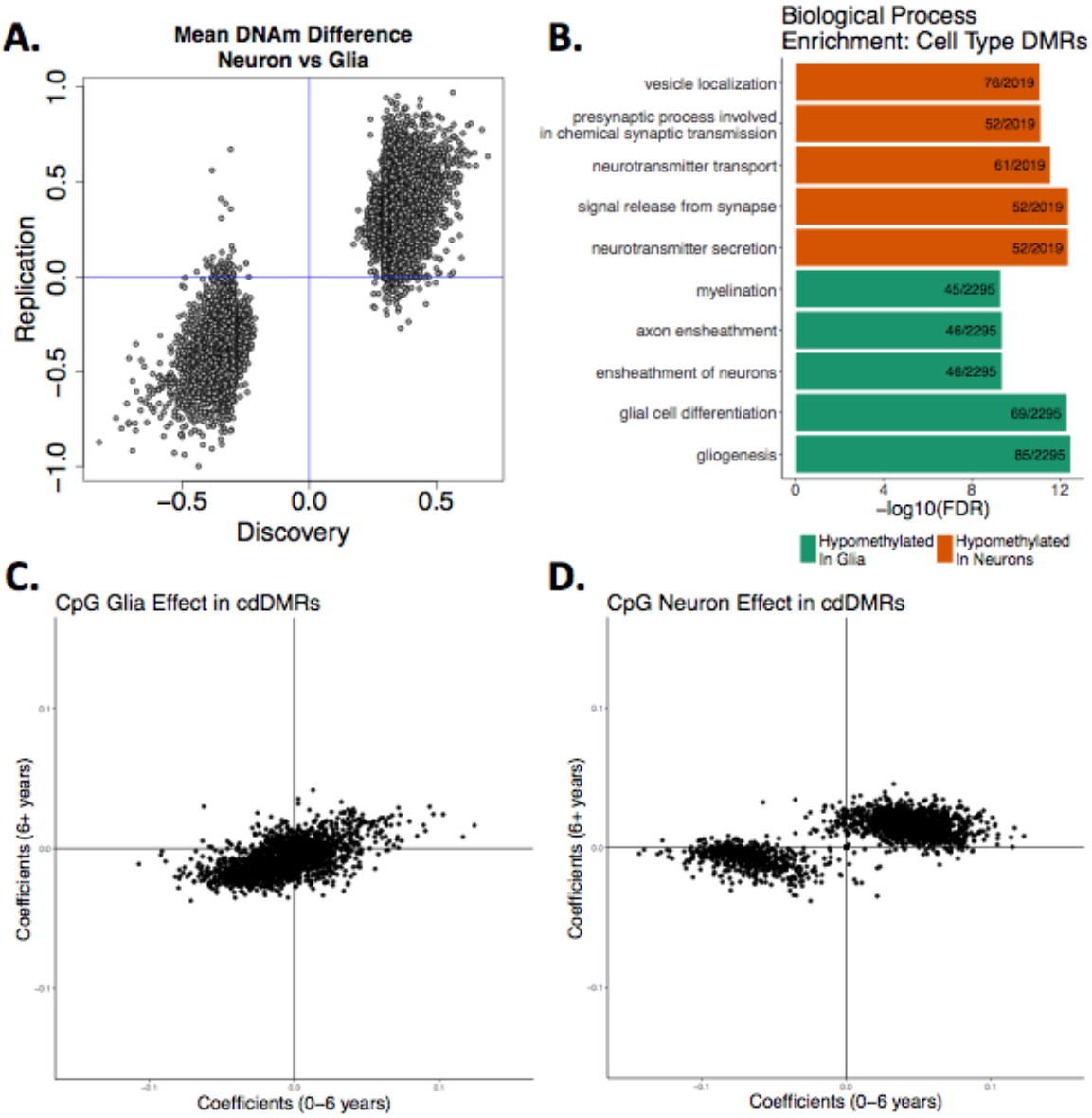

Figure S6: Differentially methylated regions (DMRs). (A) Replication of cell type DNAm differences at the CpG level between neurons and glia (NeuN+ and NeuN- samples) in our and Lister *et al.* data[1]. X and Y axes are linear model coefficients. (**B)** Enriched biological process ontology terms in the DMRs by cell type. The number of genes within each ontology group that overlaps a cell type DMR is listed. (**C)** Coefficients of linear regression on the mean mCpG level per cdDMR in samples younger than 6 years and older. **(D)** Coefficients of linear regression on the mean mCpG level per cdDMR in samples younger than 6 years and older.

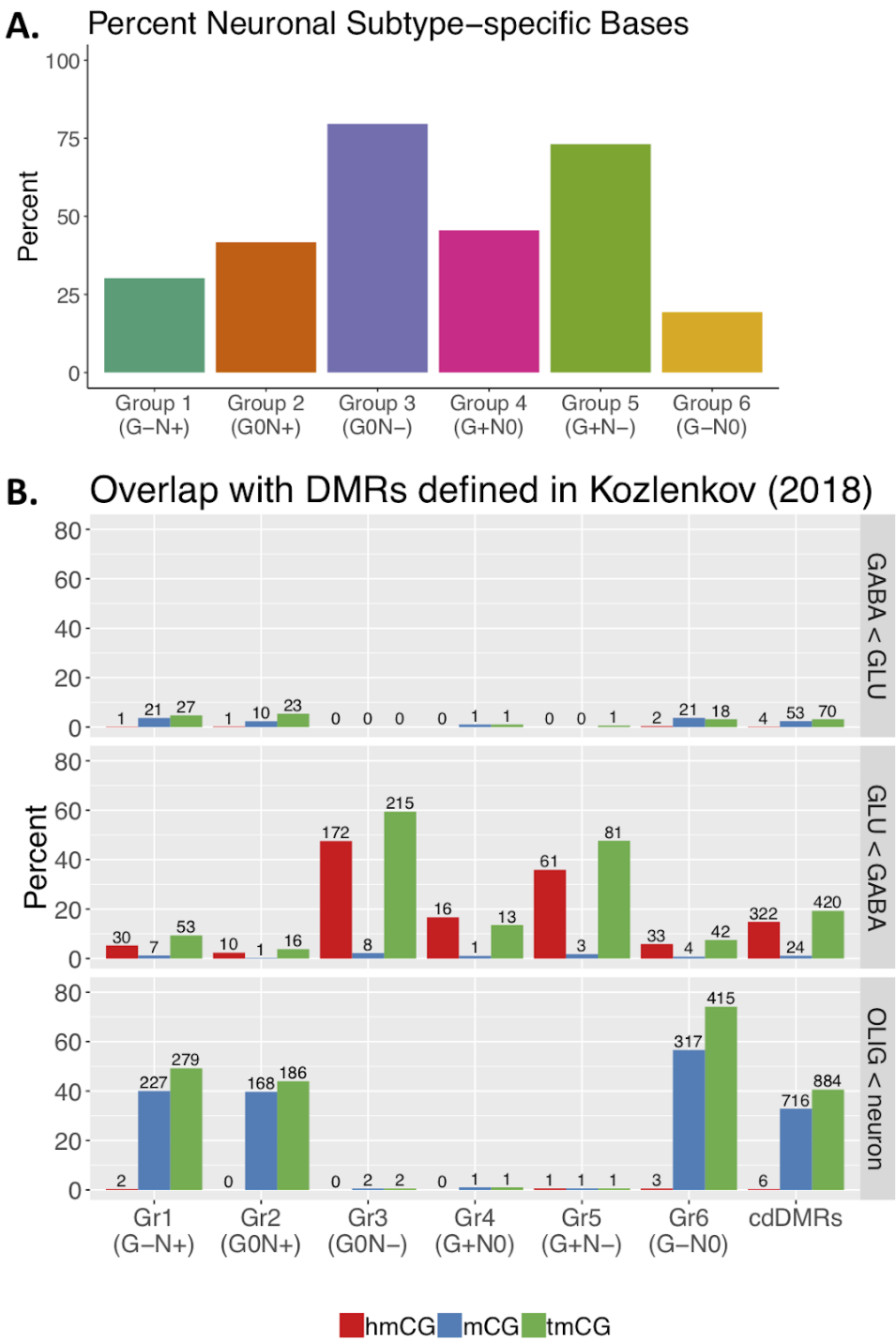

976 **Figure S7: Cell type-specific developmental DMRs and neuronal subtype methylation and**

977 **hydroxymethylation. (A)** Percent of bases within each group of cdDMRs as defined in **Figure**

978 **1B** that are differentially methylated by neuronal subtypes in Luo *et al.*[14]. **(B)** Percent of cdDMRs

979 within each of the 6 groups as defined in **Figure 1B** that overlap DMRs of methylcytosine (mC
980 captured using oxidative bisulfite sequencing), hydroxymethylcytosine (hmC), or total cytosine
981 methylation (tmC or mC+hmC, captured using standard bisulfite sequencing) as defined by
982 Kozlenkov *et al.*[50]. The plot is stratified by whether the Kozlenkov *et al.* (2018) DMRs are more
983 highly methylated in GABAergic or glutamatergic neurons, or in overall neurons compared to
984 oligodendrocytes. The number of overlapping cdDMRs are listed above each bar.

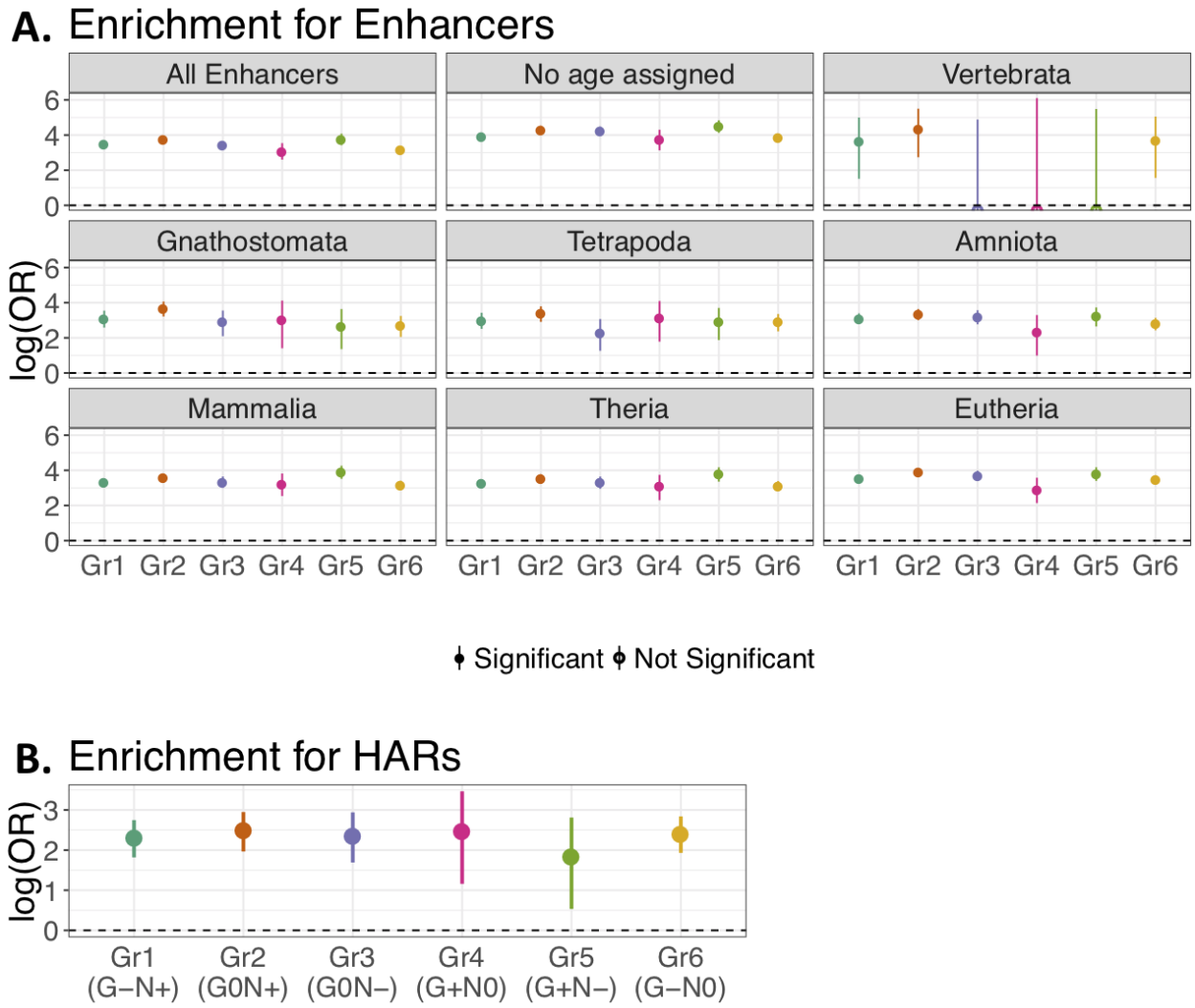

Figure S8: cdDMR overlap of human brain developmental enhancers and Human Accelerated Regions (HARs). (A) Enrichment for enhancers in the six clusters of cdDMRs from **Figure 1B** at the CpG-level. **(B)** Enrichment for human accelerated regions (HARs) in the six clusters of cdDMRs from **Figure 1B** at the CpG-level. Filled in circles indicate FDR<0.05, and error bars are the 95% confidence interval for the log(odds ratio).

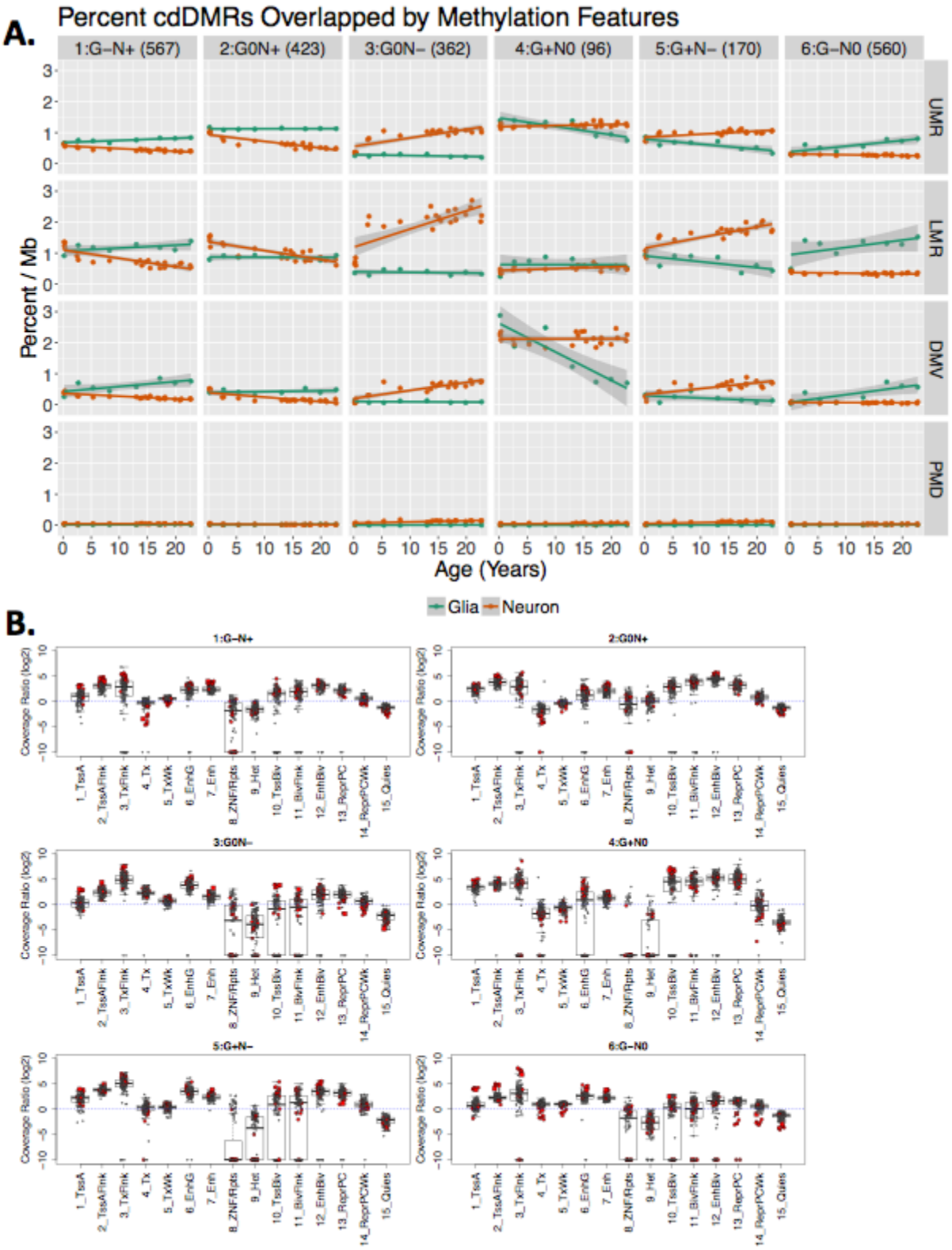

990 **Figure S9: Cell type-specific, developmentally dynamic DMRs (cdDMRs) and epigenetic**

991 **states. (A)** Percent of cdDMRs by the k-mean groups from **Figure 1B** overlapped by UMR,
992 LMR, DMV and PMD sequence across age. Lines show linear regression and shading indicates
993 the standard error. **(B)** Roadmap Epigenomics Consortium enriched chromatin states for the six
994 clusters of cdDMRs from **Figure 1B** at the CpG-level. log2(Coverage Ratio) represents the
995 enrichment of the proportion of bases within each cdDMR group in a chromatin state compared
996 to the rest of the genome.

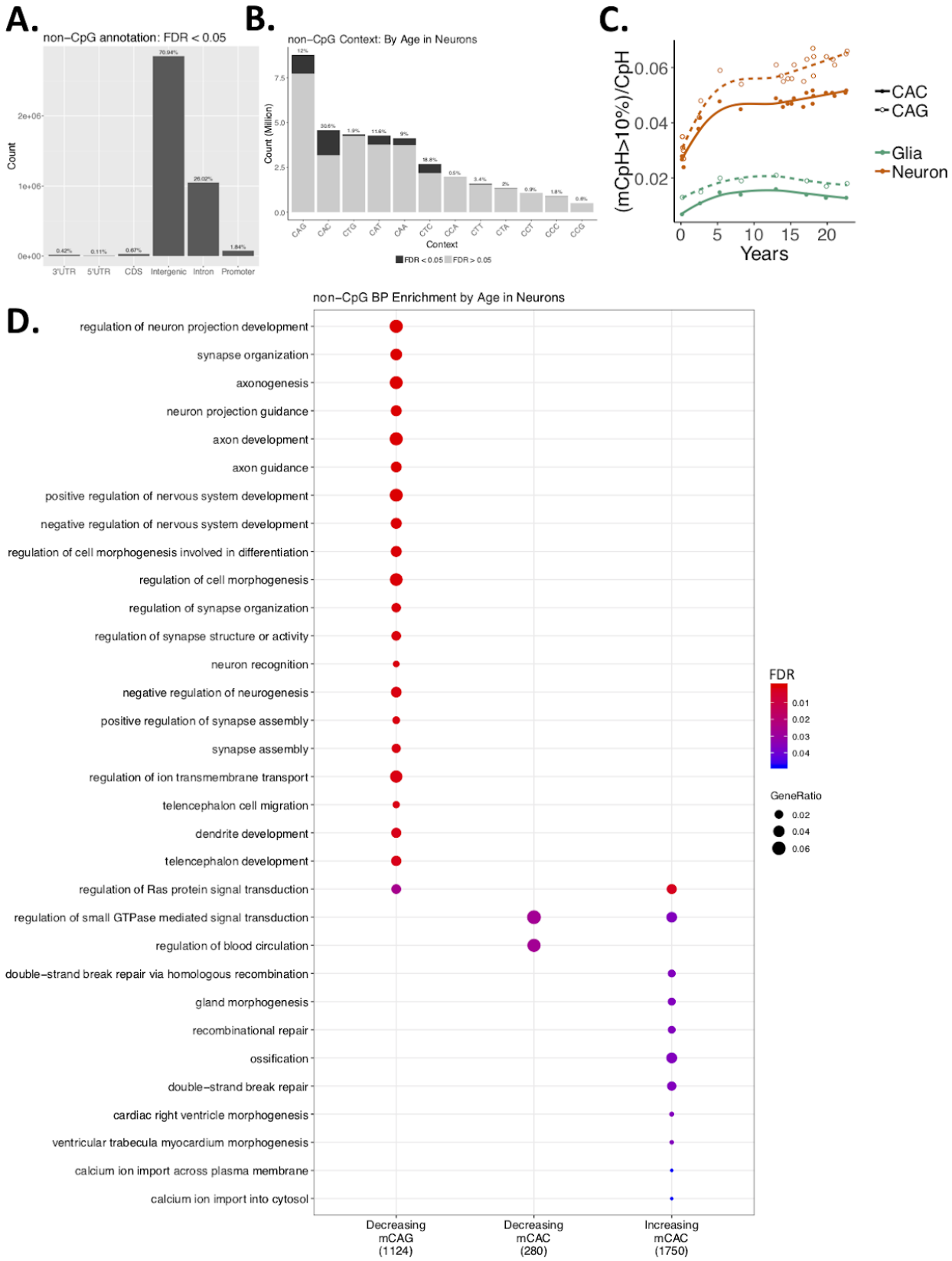
A.
non−CpG annotation: FDR < 0.05
Count
2e+06
1e+06
0e+00
0.42%
0.11%
0.67%
70.94%
26.02%
1.84%
3'UTR
5'UTR
CDS
Intergenic
Intron
Promoter
B.
non−CpG Context: By Age in Neurons
Count (Million)
7.5
5.0
2.5
0.0
12%
30.6%
1.9%
11.6%
9%
18.8%
0.5%
3.4%
2%
0.9%
1.8%
0.8%
CAG
CAC
CTG
CAT
CAA
CTC
CCA
CTT
CTA
CCT
CCC
CCG
Context
FDR < 0.05
FDR > 0.05
C.
(mCpH>10%)/CpH
0.06
0.04
0.02
0
5
10
15
20
Years
CAC
CAG
Glia
Neuron
D.
non−CpG BP Enrichment by Age in Neurons
regulation of neuron projection development
synapse organization
axonogenesis
neuron projection guidance
axon development
axon guidance
positive regulation of nervous system development
negative regulation of nervous system development
regulation of cell morphogenesis involved in differentiation
regulation of cell morphogenesis
regulation of synapse organization
regulation of synapse structure or activity
neuron recognition
negative regulation of neurogenesis
positive regulation of synapse assembly
synapse assembly
regulation of ion transmembrane transport
telencephalon cell migration
dendrite development
telencephalon development
regulation of Ras protein signal transduction
regulation of small GTPase mediated signal transduction
regulation of blood circulation
double−strand break repair via homologous recombination
gland morphogenesis
recombinational repair
ossification
double−strand break repair
cardiac right ventricle morphogenesis
ventricular trabecula myocardium morphogenesis
calcium ion import across plasma membrane
calcium ion import into cytosol
Decreasing mCAG (1124)
Decreasing mCAC (280)
Increasing mCAC (1750)
FDR
0.01
0.02
0.03
0.04
GeneRatio
0.02
0.04
0.06

997 **Figure S10: CpH methylation distribution, levels and context-specific biological process**
998 **ontology. (A)** Number of differentially methylated CpHs by cell type (FDR<5%) falling in
999 different genomic annotations across the genome. Annotation was prioritized CDS > 5'UTR >
1000 3'UTR > Intron > Promoter > Intergenic. **(B)** Breakdown of measured CpH by trinucleotide
1001 context. Differentially methylated mCpH by age in neurons (FDR<0.05) are colored in dark gray.
1002 **(C)** Accumulation of mCpH by trinucleotide context over development, stratified by cell type. **(D)**
1003 The top 20 biological process ontology terms enriched for genes exclusively overlapping CAG
1004 and CAC sites with significantly increasing or decreasing methylation levels in neurons over
1005 postnatal development (FDR<0.05).

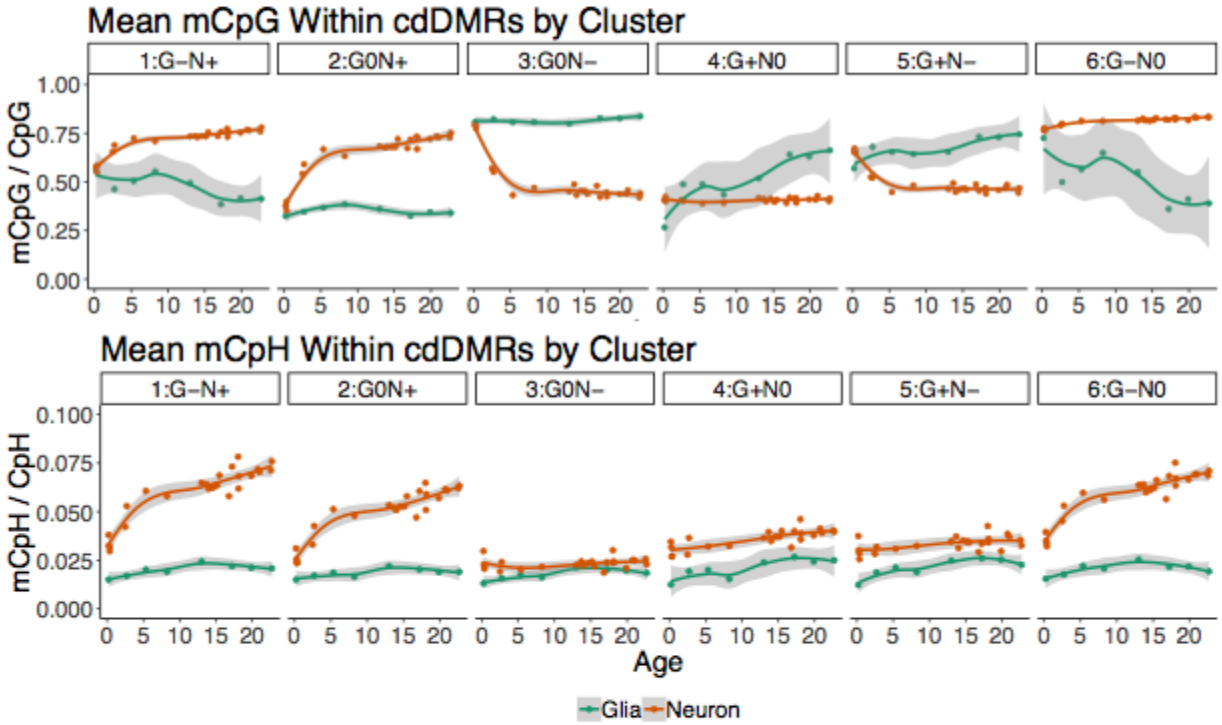

1006 **Figure S11: Trajectories of methylation accumulation in cdDMR groups.** Mean mCpH and

1007 mCpG within the cdDMRs by cluster from **Figure 1B** across development. Loess line and

1008 standard error shading are depicted.

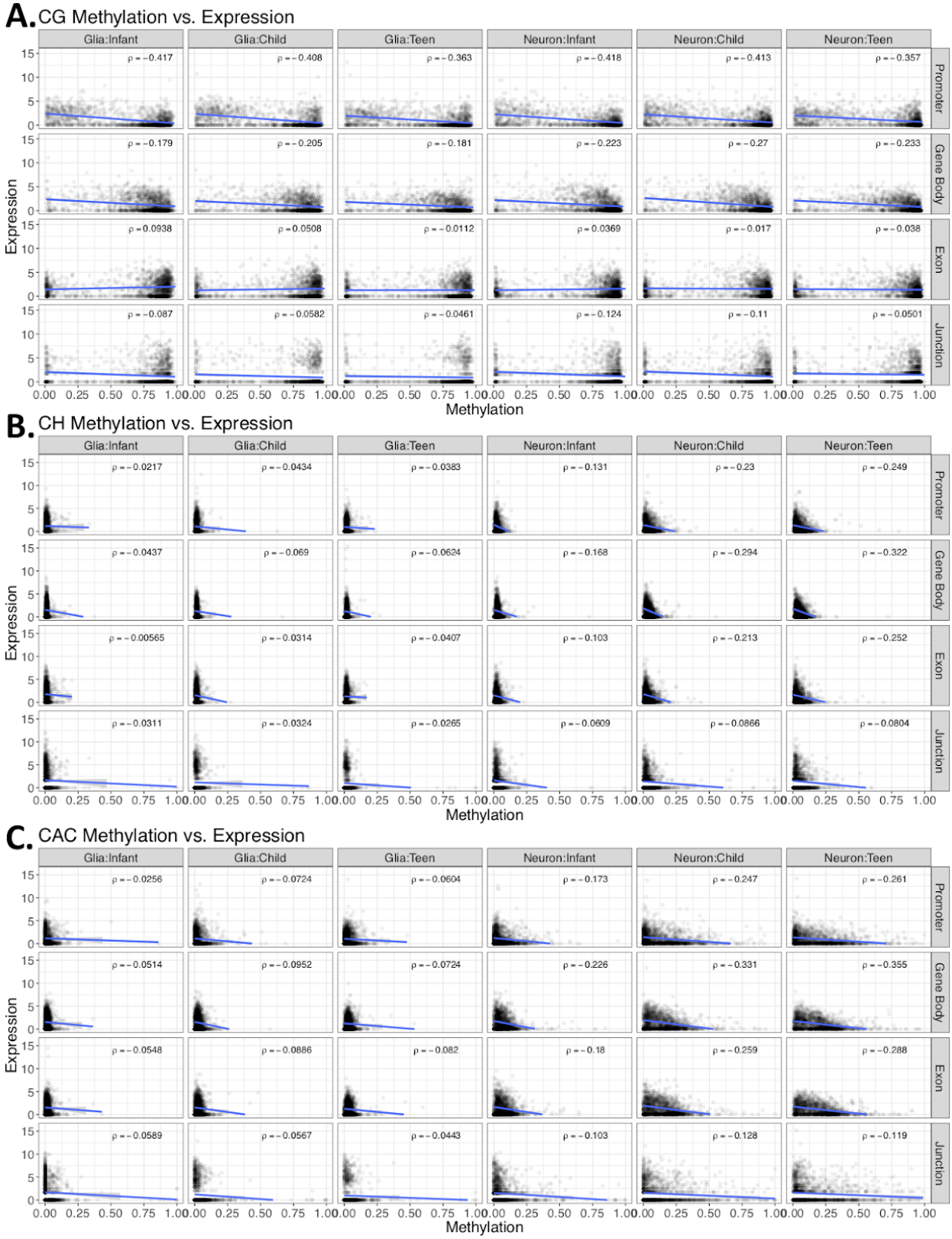
A. CG Methylation vs. Expression
Glia:Infant
Glia:Child
Glia:Teen
Neuron:Infant
Neuron:Child
Neuron:Teen
Promoter
Gene Body
Exon
Junction
Expression
Methylation
ρ = −0.417
ρ = −0.408
ρ = −0.363
ρ = −0.418
ρ = −0.413
ρ = −0.357
ρ = −0.179
ρ = −0.205
ρ = −0.181
ρ = −0.223
ρ = −0.27
ρ = −0.233
ρ = 0.0938
ρ = 0.0508
ρ = −0.0112
ρ = 0.0369
ρ = −0.017
ρ = −0.038
ρ = −0.087
ρ = −0.0582
ρ = −0.0461
ρ = −0.124
ρ = −0.11
ρ = −0.0501
B. CH Methylation vs. Expression
ρ = −0.0217
ρ = −0.0434
ρ = −0.0383
ρ = −0.131
ρ = −0.23
ρ = −0.249
ρ = −0.0437
ρ = −0.069
ρ = −0.0624
ρ = −0.168
ρ = −0.294
ρ = −0.322
ρ = −0.00565
ρ = −0.0314
ρ = −0.0407
ρ = −0.103
ρ = −0.213
ρ = −0.252
ρ = −0.0311
ρ = −0.0324
ρ = −0.0265
ρ = −0.0609
ρ = −0.0866
ρ = −0.0804
C. CAC Methylation vs. Expression
ρ = −0.0256
ρ = −0.0724
ρ = −0.0604
ρ = −0.173
ρ = −0.247
ρ = −0.261
ρ = −0.0514
ρ = −0.0952
ρ = −0.0724
ρ = −0.226
ρ = −0.331
ρ = −0.355
ρ = −0.0548
ρ = −0.0886
ρ = −0.082
ρ = −0.18
ρ = −0.259
ρ = −0.288
ρ = −0.0589
ρ = −0.0567
ρ = −0.0443
ρ = −0.103
ρ = −0.128
ρ = −0.119

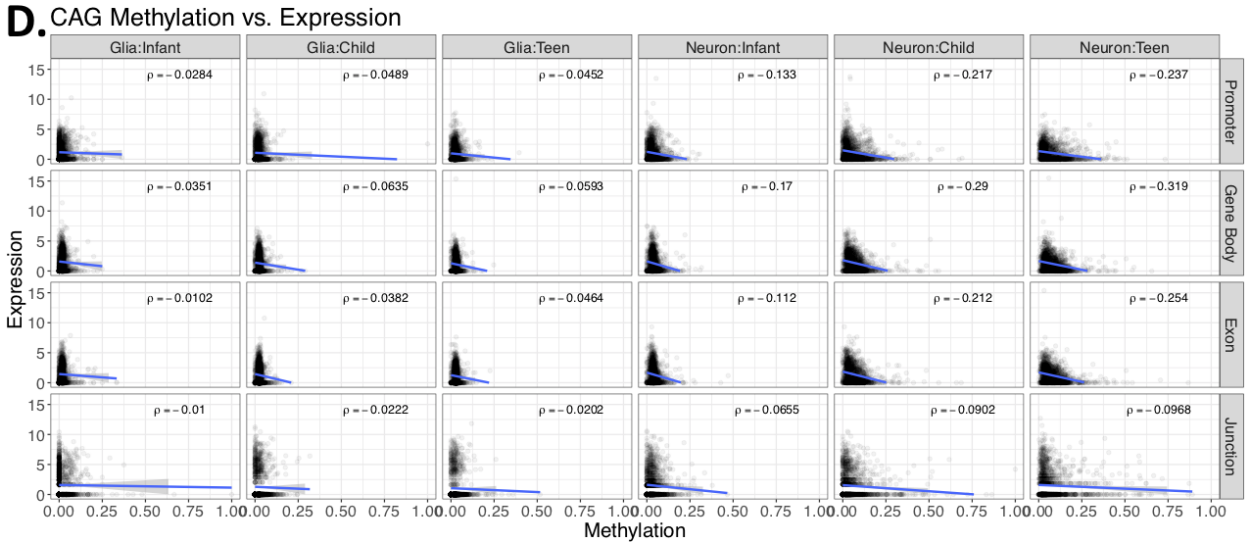

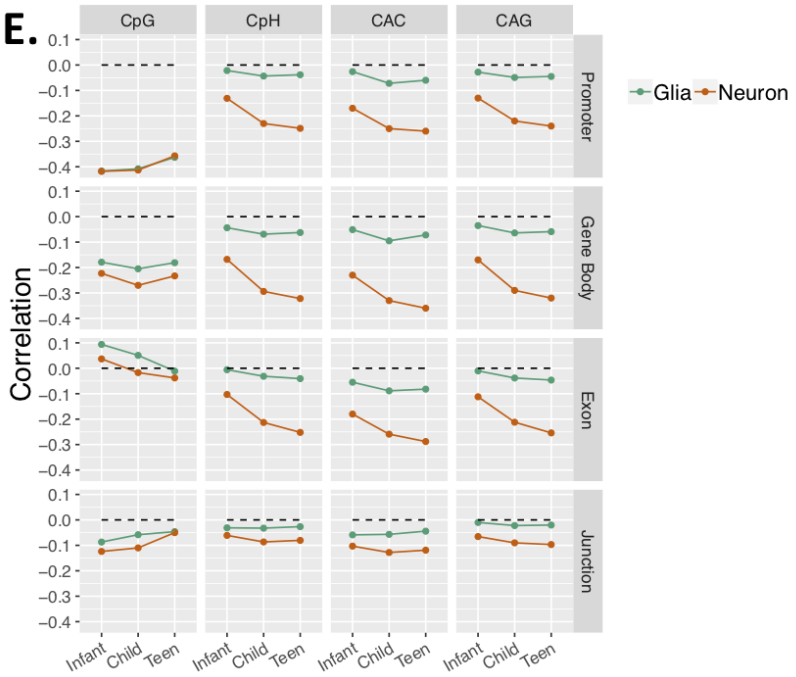

1009 **Figure S12: Relationship between methylation and expression**. **(A-D)** A random sample of
1010 10,000 expression feature:methylation pairs stratified by age and cell type in columns and
1011 feature type in rows. Each dot represents the mean methylation level of **(A)** CpGs, **(B)** CpHs,
1012 **(C)** CACs and **(D)** CAGs within the feature across all samples of that age and cell type on the
1013 x-axis and the log2([mean Rpkm]+1) for the promoters, gene bodies, and exons and the

1014 log2([mean junction-overlapping reads per 10 million mapped reads]+1) for the junctions on the
1015 y-axis. 10,000 pairs were chosen to reduce overplotting. Linear regression with shaded standard
1016 error and the rho for each correlation is listed for each plot. **(E)** Correlation of feature expression
1017 and methylation stratified by cytosine context (columns) and feature type (rows).

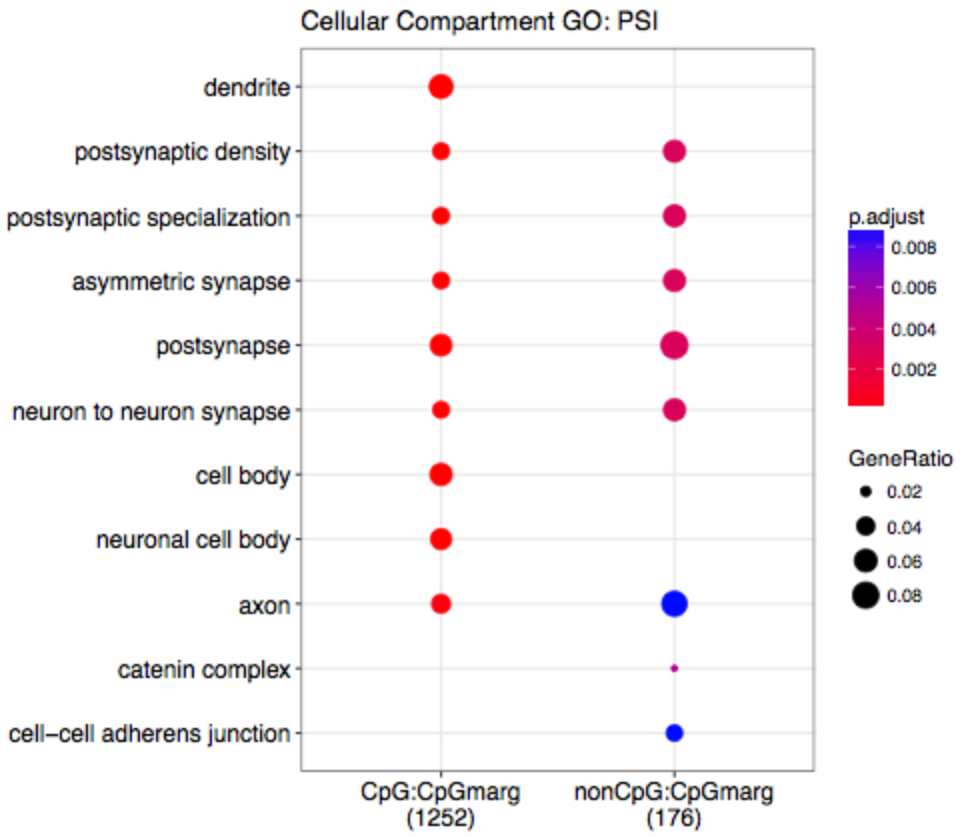

Figure S13: Cellular compartment ontology. Genes containing splicing events as measured by "percent spliced in" (PSI) that are associated with changing CpG and CpH methylation are enriched for cellular compartment gene ontology terms relating to neuronal features.

Figure S14: Molecular function ontology. Genes containing alternative exons that are associated with changing CpG and CpH methylation are enriched for molecular function ontology terms relating to neurons.

Figure S15: Web meQTL browser display. Interactive display of the CpHs and CpGs associated with expression at FDR<5% as shown at https://jhubiostatistics.shinyapps.io/wgbsExprs/. This screenshot shows the top nonCpG (mCpH) meQTL association at the gene expression level. Information about the gene is shown under *expression feature*, and information of the methylated C is shown under *cytosine*.

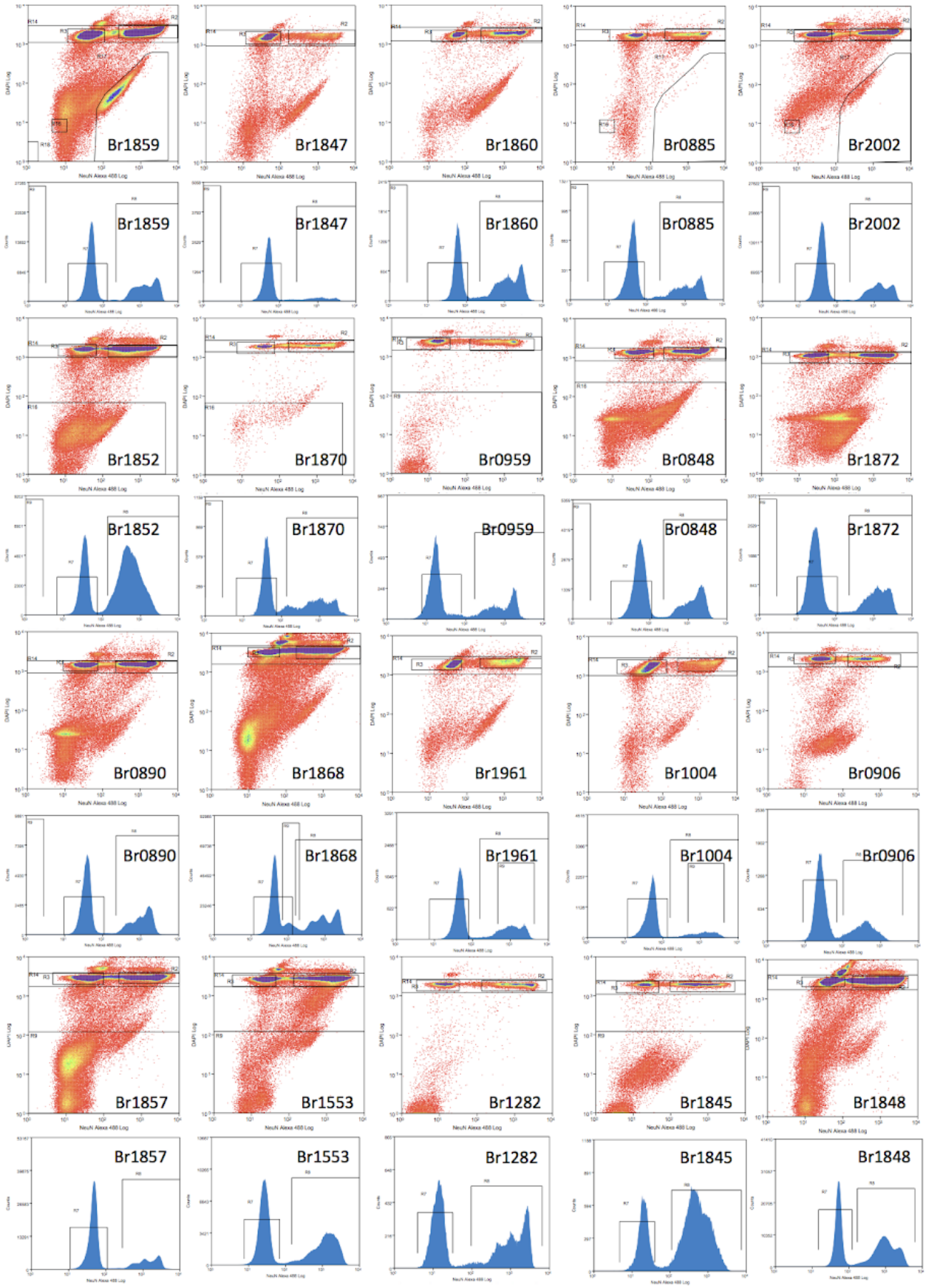
Br1859
Br1847
Br1860
Br0885
Br2002
Br1852
Br1870
Br0959
Br0848
Br1872
Br0890
Br1868
Br1961
Br1004
Br0906
Br1857
Br1553
Br1282
Br1845
Br1848

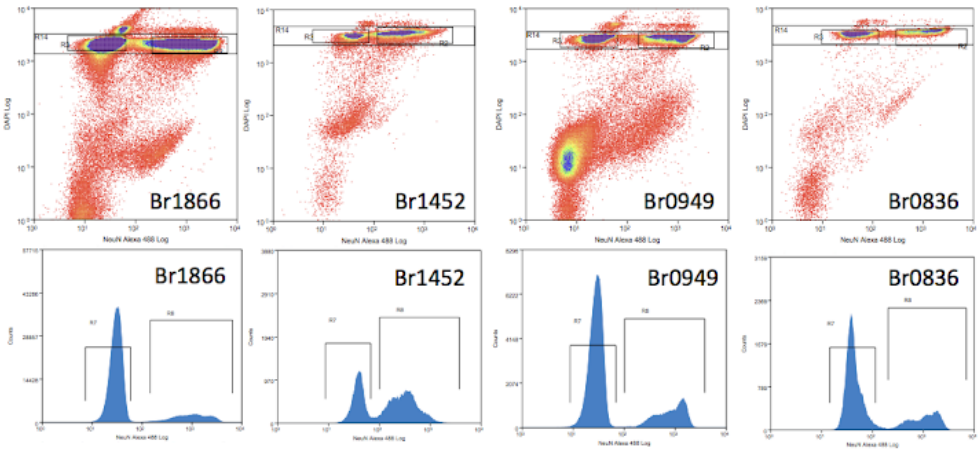

Figure S16: Raw sort data. Raw data collected from the MoFlo Legacy (Beckman Coulter) using Summit (version 4.3) software. The density plots show DAPI signal on the y-axis and Alexa Fluor 488-NeuN signal on the x-axis for events filtered via gates 1-3 as depicted in Figure S1A. The histograms show the distribution of Alexa Fluor 488-NeuN signal after including the gate for singlets based on DAPI signal (gate R14 in the raw data).

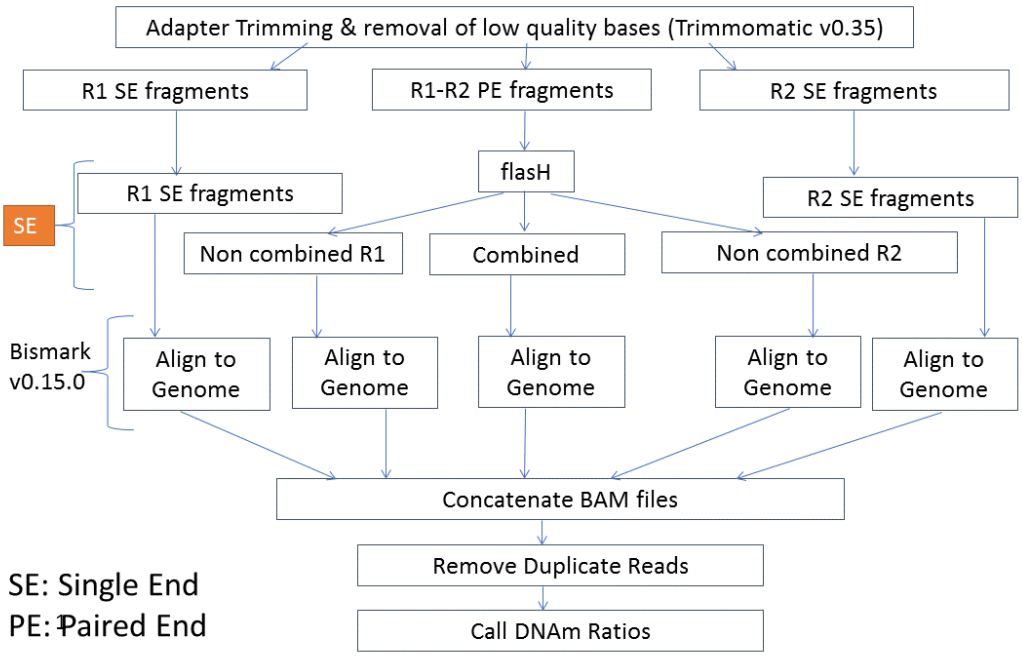

1034 **Figure S17: Data processing/alignment pipeline.** Overview of the processing steps taken to

1035 prepare the WGBS data.

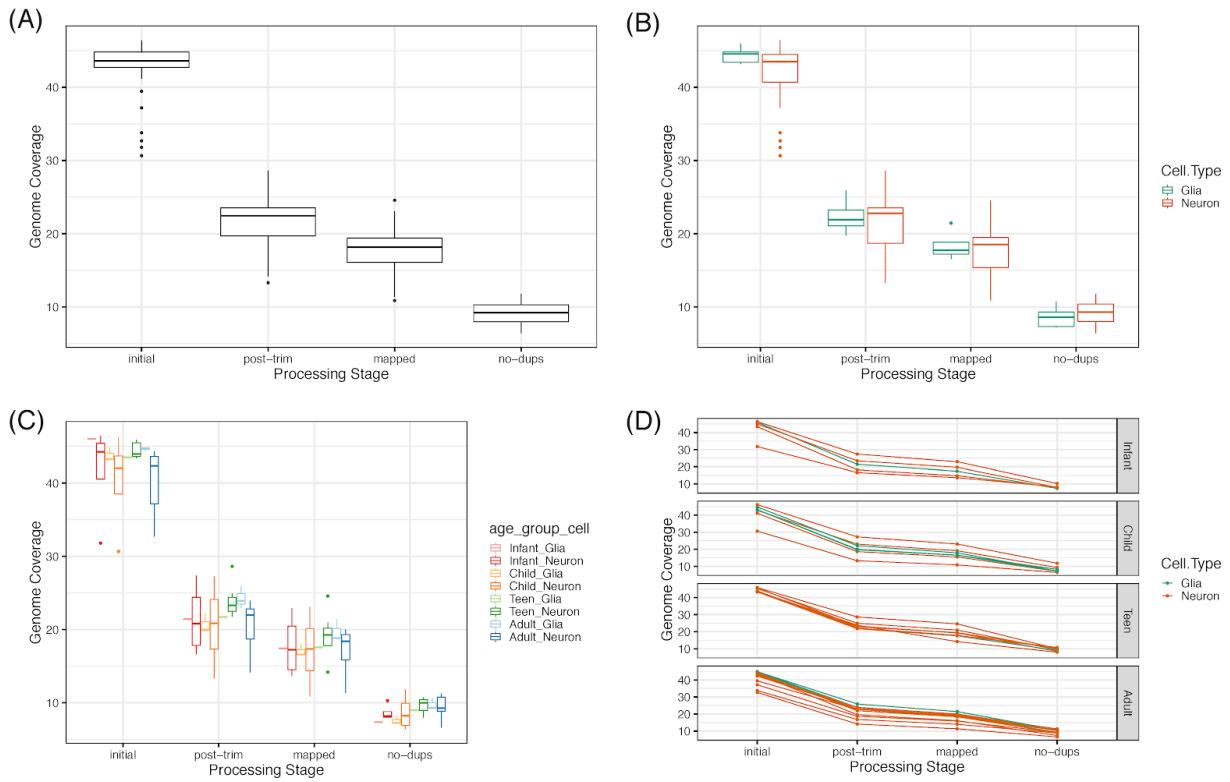

1036 **Figure S18: Genome coverage across processing stages. (A)** Genome coverage across the
1037 four main processing stages: initial FASTQ files, after trimming, after mapping to the genome,
1038 and after removing duplicated reads. **(B)** Same as (A) but with samples separated by cell type.
1039 **(C)** Genome coverage across cell types and four age categories: infant, child, teen and adult.
1040 **(D)** Genome coverage trajectories for each sample separated by age category and colored by
1041 cell type.

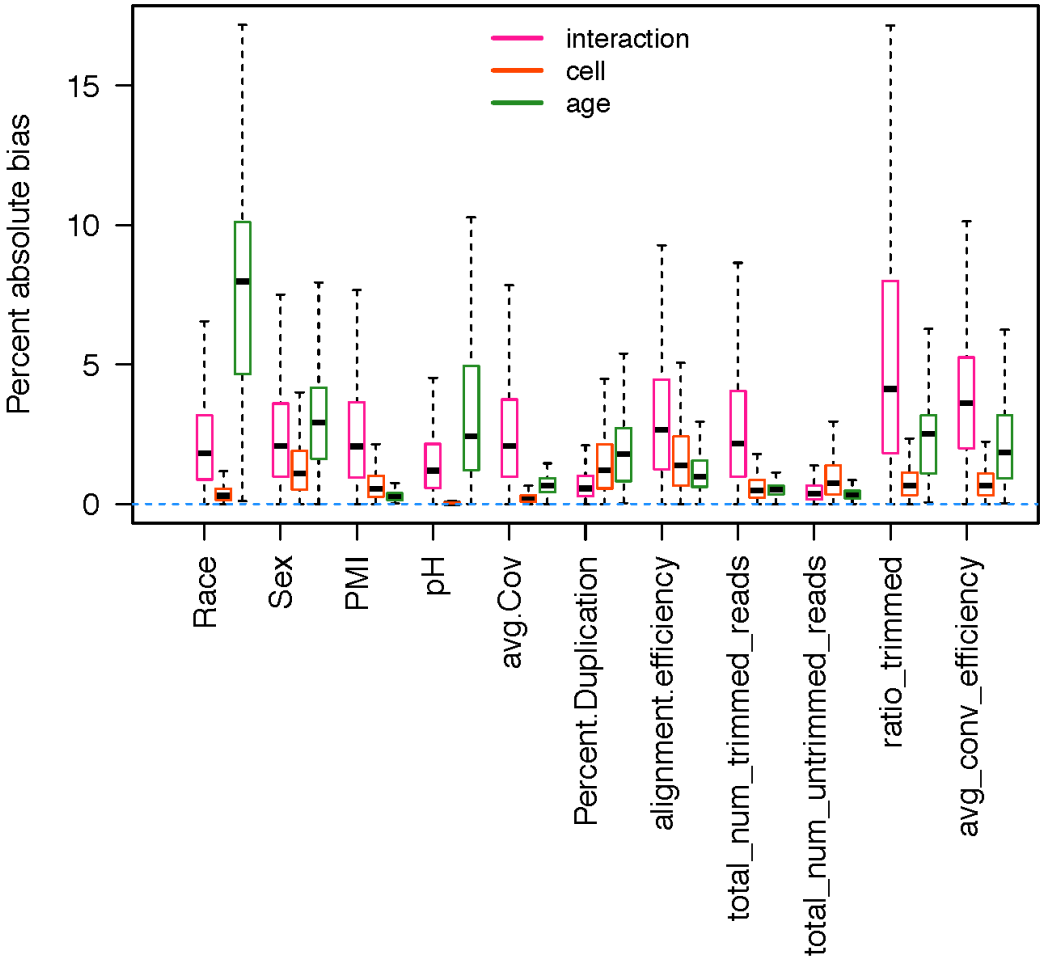

1042 **Figure S19: DMR sensitivity analyses**. This figure shows the percent absolute bias for the
1043 three coefficients of interest used to define the DMRs: age (adjusting for cell type), cell type
1044 (adjusting for age), and the interaction between age and cell type. For each DMR type we
1045 computed the coefficients after adjusting for each of the covariates in the X-axis (β_{adj}) and
1046 computed the percent absolute bias: 100 * | β_{adj} - $\beta_{original}$ | / | $\beta_{original}$ |. All covariates considered
1047 show less than 10% absolute bias. The covariates considered are: race, sex, PMI, pH, average
1048 coverage, duplication percent, alignment efficiency, total number of trimmed reads, total number
1049 of untrimmed reads, ratio of trimmed reads, and average conversion efficiency (lambda).

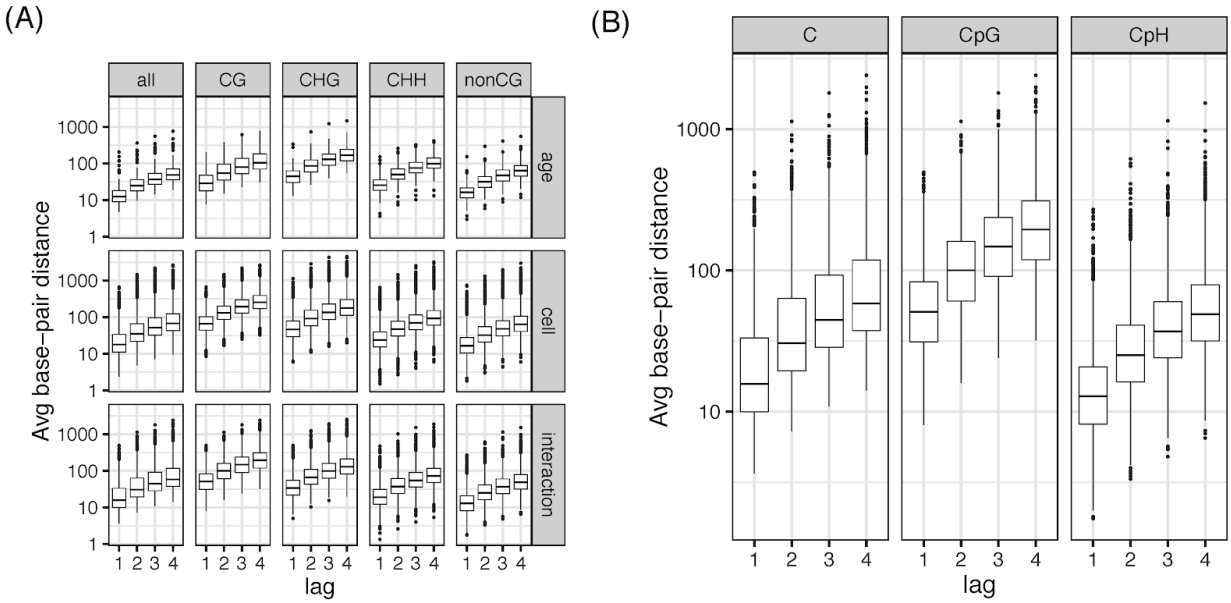

1050 **Figure S20: genome distance versus autocorrelation lag**. For each of the cytosines
1051 considered for the autocorrelation analysis in **Figure 2B**, we computed the genome base-pair
1052 distance and averaged it for each group of cytosines. **(A)** Average genomic distance for each of
1053 the three DMR models and for various contexts of cytosines. **(B)** Average genome distance for
1054 the interaction DMRs (cdDMRs) for all cytosines, CpG and CpH. The genome distance is
1055 proportional to the lag. This panel is the exact complement to **Figure 2B**.

1056 **Supplementary Tables**

1057 **Table S1: Phenotype and sequencing metrics for the WGBS samples.**

1058 *See sheet 1 of Supplementary_tables.xlsx.*

1059 **Table S2: Phenotype and sequencing metrics for the RNA-seq samples.**

1060 *See sheet 2 of Supplementary_tables.xlsx.*

1061 **Table S3: Number of cytosines measured and distribution of methylation by cytosine**

1062 **context.** Sample sizes for each sample type, number of CpGs and CpHs and distribution of

1063 CpG and CpHs across low, partial and high levels of methylation.

	N	CpG Context				CpH Context			
		# CpGs	Low (<20%)	Partial (20-80%)	High (>80%)	# CpHs	Low (<20%)	Partial (20-80%)	High (>80%)
Neuron	24	18.7×10^6	10.10%	13.90%	76.00%	58.1×10^6	91.60%	8.00%	0.40%
Glia	8	18.7×10^6	11.10%	17.80%	71.10%	58.1×10^6	99.40%	0.50%	0.10%
Fetal	20	18.7×10^6	12.10%	17.30%	70.60%	58.1×10^6	99.75%	0.17%	0.07%
Homogenate	23	28.2×10^6	8.50%	16.90%	73.70%	58.1×10^6	*NA*	*NA*	*NA*

1064 **Table S4: Cell type-specific, developmental differentially methylated regions (cdDMRs).**

1065 *See sheet 4 of Supplementary_tables.xlsx.*

1066 **Table S5: mC association with cell type and age in postnatal cell type-specific samples.**

1067 Number of differentially methylated CpGs and CpHs across each of the statistical models: cell

1068 type effects adjusting for age, age effects adjust for cell type, cell type and age interaction

1069 effects, as well as age in neuron samples only.

Model	CpG Context		CpH Context	
	FDR ≤ 0.05	% Significant	FDR ≤ 0.05	% Significant
Cell type	4824804	25.80%	7682075	18.80%
Age	536164	2.90%	3194618	7.80%
Cell type:Age	90227	0.50%	76	0%
Age in Neurons	*NA*	*NA*	4020371	9.80%

1070 **Table S6: GWAS traits assessed using LDSC.**

1071 *See sheet 6 of Supplementary_tables.xlsx.*

1072 **Table S7: Stratified linkage disequilibrium score regression results.**

1073 *See sheet 7 of Supplementary_tables.xlsx.*

1074 **Table S8: Enrichment of DMRs and mCpH for disease-associated gene sets.**

1075 *See sheet 8 of Supplementary_tables.xlsx.*

1076 **Table S9: Enrichment for disease gene sets in DNAm-splicing association features.**

1077 *See sheet 9 of Supplementary_tables.xlsx.*

1078 **Table S10: Variable dictionary for Table 1**. Variables used in **Table 1** with their full definition.

Variable	Description
Feature	Either gene, exon or event affect the percent spliced in (PSI).
Methylation	Methylation type. Either CpG or CpH.
Direction	down.
N	Number of associations at FDR 5%.
N Unique C	Number of unique cytosines in these associations.
N Unique Features	Number of unique features in these associations.
N Meth>0	Mean number of samples that have non-zero methylation values. Total 22.
N Meth<1	Mean number of samples that have non-one methylation values.
Expr Change	Mean change in expression (ignoring NAs).
Age Confounded	Proportion of associations that are confounded by age, that is, proportion of associations where the methylation coefficient in a multiple linear regression adjusting for age has a FDR >= 5%.
Promoter	Proportion of cytosines in these associations that overlap gene promoters. A single cytosine can overlap multiple gene regions for different genes.
Gene Body	Proportion of cytosines in these associations that overlap gene bodies.
Gene Flanking	Proportion of cytosines in these associations that overlap gene flanking regions.
CHG	Proportion of cytosines in these associations that have a CHG context.
CHH	Proportion of cytosines in these associations that have a CHH context.
Glia	Proportion of features in these associations where the feature is differentially expressed between neurons and glia, with higher expression in glia. For genes and PSI, the gene list was used. Up to the top 5,000 features DE in each direction were used.
Neuron	Proportion of features in these associations where the feature is differentially expressed between neurons and glia, with higher expression in neurons.
No Diff	Proportion of features in outside the top differentially expressed genes between glia and neuron.

1079 **Bibliography**

1080 1. Lister, R. *et al.* Global epigenomic reconfiguration during mammalian brain development.
1081 *Science* **341,** 1237905 (2013).
1082 2. Jaffe, A. E. *et al.* Mapping DNA methylation across development, genotype and
1083 schizophrenia in the human frontal cortex. *Nat. Neurosci.* **19,** 40–47 (2016).
1084 3. Jaffe, A. E. & Irizarry, R. A. Accounting for cellular heterogeneity is critical in
1085 epigenome-wide association studies. *Genome Biol.* **15,** R31 (2014).
1086 4. Schultz, M. D. *et al.* Human body epigenome maps reveal noncanonical DNA methylation
1087 variation. *Nature* **523,** 212–216 (2015).
1088 5. Mo, A. *et al.* Epigenomic signatures of neuronal diversity in the mammalian brain. *Neuron*
1089 **86,** 1369–1384 (2015).
1090 6. Jeong, M. *et al.* Large conserved domains of low DNA methylation maintained by Dnmt3a.
1091 *Nat. Genet.* **46,** 17–23 (2014).
1092 7. Xie, W. *et al.* Epigenomic analysis of multilineage differentiation of human embryonic stem
1093 cells. *Cell* **153,** 1134–1148 (2013).
1094 8. Stadler, M. B. *et al.* DNA-binding factors shape the mouse methylome at distal regulatory
1095 regions. *Nature* **480,** 490–495 (2011).
1096 9. Lister, R. *et al.* Human DNA methylomes at base resolution show widespread epigenomic
1097 differences. *Nature* **462,** 315–322 (2009).
1098 10. Salhab, A. *et al.* Partially methylated domains are hallmarks of a cell specific epigenome
1099 topology. *BioRxiv* (2018). doi:10.1101/249334
1100 11. Hovestadt, V. *et al.* Decoding the regulatory landscape of medulloblastoma using DNA
1101 methylation sequencing. *Nature* **510,** 537–541 (2014).
1102 12. Roadmap Epigenomics Consortium *et al.* Integrative analysis of 111 reference human

1103 epigenomes. *Nature* **518,** 317–330 (2015).
1104 13. Zhou, W. *et al.* DNA methylation loss in late-replicating domains is linked to mitotic cell
1105 division. *Nat. Genet.* **50,** 591–602 (2018).
1106 14. Luo, C. *et al.* Single-cell methylomes identify neuronal subtypes and regulatory elements in
1107 mammalian cortex. *Science* **357,** 600–604 (2017).
1108 15. Emera, D., Yin, J., Reilly, S. K., Gockley, J. & Noonan, J. P. Origin and evolution of
1109 developmental enhancers in the mammalian neocortex. *Proc Natl Acad Sci USA* **113,**
1110 E2617-26 (2016).
1111 16. Doan, R. N. *et al.* Mutations in human accelerated regions disrupt cognition and social
1112 behavior. *Cell* **167,** 341–354.e12 (2016).
1113 17. He, Y. & Ecker, J. R. Non-CG Methylation in the Human Genome. *Annu. Rev. Genomics*
1114 *Hum. Genet.* **16,** 55–77 (2015).
1115 18. Eckhardt, F. *et al.* DNA methylation profiling of human chromosomes 6, 20 and 22. *Nat.*
1116 *Genet.* **38,** 1378–1385 (2006).
1117 19. Shukla, S. *et al.* CTCF-promoted RNA polymerase II pausing links DNA methylation to
1118 splicing. *Nature* **479,** 74–79 (2011).
1119 20. Rizzardi, L. F. *et al.* Neuronal brain-region-specific DNA methylation and chromatin
1120 accessibility are associated with neuropsychiatric trait heritability. *Nat. Neurosci.* **22,**
1121 307–316 (2019).
1122 21. Brainstorm Consortium *et al.* Analysis of shared heritability in common disorders of the
1123 brain. *Science* **360,** (2018).
1124 22. Finucane, H. K. *et al.* Partitioning heritability by functional annotation using genome-wide
1125 association summary statistics. *Nat. Genet.* **47,** 1228–1235 (2015).
1126 23. Skene, N. G. *et al.* Genetic identification of brain cell types underlying schizophrenia. *Nat.*

1127 *Genet.* **50,** 825–833 (2018).

1128 24. Birnbaum, R., Jaffe, A. E., Hyde, T. M., Kleinman, J. E. & Weinberger, D. R. Prenatal
1129 expression patterns of genes associated with neuropsychiatric disorders. *Am. J. Psychiatry*
1130 **171,** 758–767 (2014).

1131 25. Schizophrenia Working Group of the Psychiatric Genomics Consortium. Biological insights
1132 from 108 schizophrenia-associated genetic loci. *Nature* **511,** 421–427 (2014).

1133 26. Howell, K. R., Floyd, K. & Law, A. J. PKBγ/AKT3 loss-of-function causes learning and
1134 memory deficits and deregulation of AKT/mTORC2 signaling: Relevance for schizophrenia.
1135 *PLoS ONE* **12,** e0175993 (2017).

1136 27. Wang, D. *et al.* Comprehensive functional genomic resource and integrative model for the
1137 human brain. *Science* **362,** (2018).

1138 28. Stiles, J. & Jernigan, T. L. The basics of brain development. *Neuropsychol. Rev.* **20,**
1139 327–348 (2010).

1140 29. Tierney, A. L. & Nelson, C. A. Brain development and the role of experience in the early
1141 years. *Zero Three* **30,** 9–13 (2009).

1142 30. Stroud, H. *et al.* Early-Life Gene Expression in Neurons Modulates Lasting Epigenetic
1143 States. *Cell* **171,** 1151–1164.e16 (2017).

1144 31. Lev Maor, G., Yearim, A. & Ast, G. The alternative role of DNA methylation in splicing
1145 regulation. *Trends Genet.* **31,** 274–280 (2015).

1146 32. Jaffe, A. E. *et al.* Developmental and genetic regulation of the human cortex transcriptome
1147 illuminate schizophrenia pathogenesis. *Nat. Neurosci.* **21,** 1117–1125 (2018).

1148 33. Kozlenkov, A. *et al.* Substantial DNA methylation differences between two major neuronal
1149 subtypes in human brain. *Nucleic Acids Res.* **44,** 2593–2612 (2016).

1150 34. Sahara, S., Yanagawa, Y., O'Leary, D. D. M. & Stevens, C. F. The fraction of cortical

GABAergic neurons is constant from near the start of cortical neurogenesis to adulthood. *J. Neurosci.* **32,** 4755–4761 (2012).

35. Kozlenkov, A. *et al.* A unique role for DNA (hydroxy)methylation in epigenetic regulation of human inhibitory neurons. *Sci. Adv.* **4,** eaau6190 (2018).
36. Lipska, B. K. *et al.* Critical factors in gene expression in postmortem human brain: Focus on studies in schizophrenia. *Biol. Psychiatry* **60,** 650–658 (2006).
37. Krueger, F. & Andrews, S. R. Bismark: a flexible aligner and methylation caller for Bisulfite-Seq applications. *Bioinformatics* **27,** 1571–1572 (2011).
38. Bolger, A. M., Lohse, M. & Usadel, B. Trimmomatic: a flexible trimmer for Illumina sequence data. *Bioinformatics* **30,** 2114–2120 (2014).
39. Magoč, T. & Salzberg, S. L. FLASH: fast length adjustment of short reads to improve genome assemblies. *Bioinformatics* **27,** 2957–2963 (2011).
40. Langmead, B. & Salzberg, S. L. Fast gapped-read alignment with Bowtie 2. *Nat. Methods* **9,** 357–359 (2012).
41. Li, H. *et al.* The Sequence Alignment/Map format and SAMtools. *Bioinformatics* **25,** 2078–2079 (2009).
42. Hansen, K. D., Langmead, B. & Irizarry, R. A. BSmooth: from whole genome bisulfite sequencing reads to differentially methylated regions. *Genome Biol.* **13,** R83 (2012).
43. Jaffe, A. E. *et al.* Bump hunting to identify differentially methylated regions in epigenetic epidemiology studies. *Int. J. Epidemiol.* **41,** 200–209 (2012).
44. Ritchie, M. E. *et al.* limma powers differential expression analyses for RNA-sequencing and microarray studies. *Nucleic Acids Res.* **43,** e47 (2015).
45. Morgan, M. *AnnotationHub: Client to access AnnotationHub resources*. (Bioconductor, 2019). at <http://bioconductor.org/packages/release/bioc/html/AnnotationHub.html>

46. Kim, D., Langmead, B. & Salzberg, S. L. HISAT: a fast spliced aligner with low memory requirements. *Nat. Methods* **12,** 357–360 (2015).

47. Liao, Y., Smyth, G. K. & Shi, W. featureCounts: an efficient general purpose program for assigning sequence reads to genomic features. *Bioinformatics* **30,** 923–930 (2014).

48. Goldstein, L. D. *et al.* Prediction and Quantification of Splice Events from RNA-Seq Data. *PLoS ONE* **11,** e0156132 (2016).

49. Robinson, M. D., McCarthy, D. J. & Smyth, G. K. edgeR: a Bioconductor package for differential expression analysis of digital gene expression data. *Bioinformatics* **26,** 139–140 (2010).

50. Law, C. W., Chen, Y., Shi, W. & Smyth, G. K. voom: Precision weights unlock linear model analysis tools for RNA-seq read counts. *Genome Biol.* **15,** R29 (2014).

51. Yu, G., Wang, L.-G., Han, Y. & He, Q.-Y. clusterProfiler: an R package for comparing biological themes among gene clusters. *OMICS* **16,** 284–287 (2012).

52. Shabalin, A. A. Matrix eQTL: ultra fast eQTL analysis via large matrix operations. *Bioinformatics* **28,** 1353–1358 (2012).